PARTICLE SIZE REDUCTION IN GEOPHYSICAL GRANULAR FLOWS:

THE ROLE OF ROCK FRAGMENTATION

A Thesis submitted to the faculty of

San Francisco State University

In partial fulfillment of

the requirements for

the Degree

Master of Science

In

Geoscience

by

Gionata Bianchi

San Francisco, California
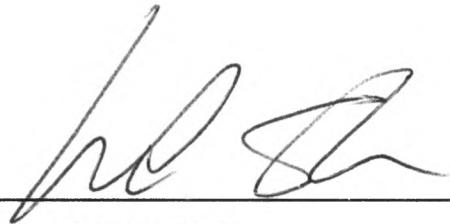
May 2017

CERTIFICATION OF APPROVAL
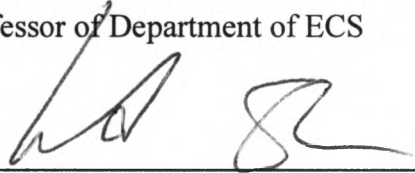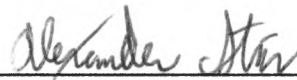
I certify that I have read *Particle Size Reduction in Geophysical Granular Flows: The Role of Rock Fragmentation* by Gionata Bianchi, and that in my opinion this work meets the criteria for approving a thesis submitted in partial fulfillment of the requirement for the degree Master of Science in Geosciences at San Francisco State University.

Leonard Sklar, Ph.D.
Professor of Department of ECS

Jason Gurdak, Ph.D.
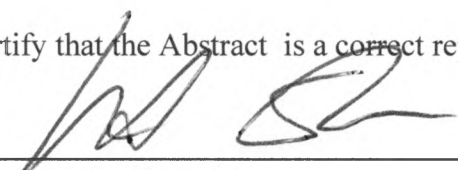Associate Professor of Department of ECS

Alexander Stine, Ph.D.
Assistant Professor of Department of ECS

PARTICLE SIZE REDUCTION IN GEOPHYSICAL GRANULAR FLOWS: THE ROLE OF ROCK FRAGMENTATION
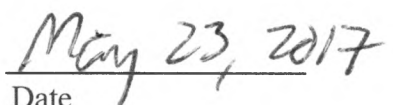
Gionata Bianchi

San Francisco, California

2017

Particle size reduction in geophysical granular flows is caused by abrasion and fragmentation. Controls on fragmentation are not well understood. In this study, I used laboratory experiments to measure fragmentation probability and resulting fragment sizes, to calibrate a numerical model that can predict how particle size distributions evolve with travel distance in laboratory drums and in the field. Using free-fall single-particle experiments with granodiorite, basalt and serpentinite samples, I found that fragmentation probability is a power function of impact energy, with an exponent that varies between 0.66 and 1.03 for different rock types. I also found that fragment size distributions can be represented with a single power relationship for each rock type, independent of impact energy. These results were used to calibrate a numerical code that simulates the production and size evolution of sediment particles by fragmentation and abrasion. I tested the code using particle size measurements from rotating drum experiments that physically model granular flows in nature. In a related project, I documented down-valley fining of debris flow deposits at Inyo Creek, California, which may result from particle fragmentation during high energy particle interactions.

I certify that the Abstract is a correct representation of the content of this thesis.

_____   _____

Chair, Thesis Committee   Date

ACKNOWLEDGEMENTS

TABLE OF CONTENTS

LIST OF TABLES

LIST OF FIGURES

1.0 Introduction

Geophysical granular flows are dense fluid-particle flows in which the particle-particle interactions are a dominant feature. Pyroclastic flows, snow avalanches, and debris flows are examples of geophysical granular flows. Debris flows are highly concentrated dispersions of poorly sorted sediment (clay to boulder size particles) in water, which can move at speeds greater than 10 m/s, discharge volumes as large as 10^9 m^3, and release more than 10^{16} J of energy (Arattano and Marchi, 2008; Iverson, 1997). Debris flows can occur anywhere along steep, hilly and mountainous slopes. Debris flows typically originate from landslides on slopes steeper than 30 degrees, under intense rain or snowmelt conditions. They can also be caused by rock avalanches or other types of mass wasting that acquire the characteristic percentage of fines (3% by weight mud) during their run downstream (Arabnia, 2015). Landslides and resulting debris flows kill between 25 to 50 people and cause 3.5 billion dollars in damage in the United States of America annually (Highland and Johnson, 2014). The distance travelled before the flow stops is influenced by the particle size distribution (PSD) within the flow, especially by the finer sediments in the fluid part (silt and clay) (Bowman et al., 2012). The PSD in debris flows evolves because of fragmentation and abrasion (Kuenen, 1956), and because of the deposition and entrainment of particles from bed material or collapse of stream banks.

Particle size reduction in debris flows should be influenced by rock strength, energy of transport, pore pressure inside the flow, and the type of particle wear (Arabnia, 2015; Montserrat et al., 2012). Particle wear can be divided into two types, the chipping off of tiny silt sized particles (abrasion), and fracturing that produces larger fragments (fragmentation). Abrasion in debris flows may be modeled the same way as particle abrasion in fluvial environment. The fining of sediment in fluvial channels was first described by Sternberg (1875) through the equation:

$$D = D_0 e^{-\alpha_D x}$$ eqn.1

where D is the grain size [L], D_0 is the initial grain size [L], α_D is the abrasion coefficient [(L/L)/L], and x is the distance traveled by the sediment [L]. Equation 1 can be modified to calculate the loss in weight of sediment over distance:

$$M = M_0 e^{-\alpha_M x}$$ eqn.2

where M is the mass or bulk mass of one or multiple particles [M], M_0 is the initial mass of particles [M], and $\alpha_M = 3\alpha_D$ assuming spherical particles. The Sternberg model (eqns. 1 and 2) has been used consistently in the literature for fluvial abrasion, however there is still considerable uncertainty surrounding the controls on α_D (Arabnia, 2015). Moreover, this approach does not account for the creation of new particles by fragmentation. Because debris flows create high energy interactions between particles, fragmentation may be particularly important in particle size evolution in that environment. While eqn. 1 provides some predictive ability for abrasion, there are important unanswered questions

on the controls of fragmentation, including how best to model fragmentation processes, and isolate and quantify the relative importance of fragmentation from other erosional phenomena.

Debris flows are challenging to study in the field because of their extreme violence. Consequently, laboratory experiments are fundamental for studying the physics underlying these phenomena. A variety of laboratory experiments to simulate debris flows have been reported in the literature. Debris flow flumes (Iverson et al., 2010) and rotating drums (Arabnia, 2015; Hsu et al., 2014; Kaitna et al., 2014) have been used to study rheology and physics in a more controlled and simplified environment than in the field. Rotating drums are particularly appealing because of the possibility to have longer, and more realistic transport distances than debris flow flumes. Furthermore, abrasion and fragmentation rates can be measured after longer time intervals allowing a better understanding of the factors influencing flow evolution.

Le Bouteiller et al. (2011) developed a theoretical model that can be used for predicting particle size evolution due to fragmentation and abrasion. They used a method for direct study of fragmentation that consists of dropping rock particles in the air above a hard surface and measuring the frequency and outcome of fragmentation events (Figure 1). They found that the impact velocity and the initial surface state (which they represent with a "fissuration" index) are the main parameters influencing fragmentation, while

other factors such as whether the particles have been saturated in water, the particle mass, and number of previous impacts, are not statistically significant in the material degradation (Le Bouteiller et al., 2010). All their conclusions were made based on experiments with a small dataset of drops, using marl particles.

This study builds on the work of Le Bouteiller et al. (2010) and previous research by Arabnia (2015), Arabnia et al. (2015a, 2015b), and Arabnia and Sklar (2015), who created granular flows in four drums, with diameters ranging from 0.2 m to 4 m (Figure 2). That work showed that the size distributions of new coarse particles produced by fragmentation have a shape well-represented by a three-parameter Weibull distribution. Sediment dynamics in rotating drums can be scaled to field conditions using non-dimensional numbers to achieve geometric and dynamic similarity (Hsu et al., 2008; Schneider et al., 2011). However, there is a threshold rate of energy expenditure, or power, at which fragmentation becomes negligible and abrasion is dominant for drum experiments. As observed by Arabnia (2015), fragmentation was significant only for the large drum (4 m diameter) and does not scale with power, while mass loss to fines (sand and silt), and the variation in fine sediment concentration, do scale with drum power.

To scale fragmentation from drop experiments to the field, I chose to use drop experiments to measure the fragmentation probability. Furthermore, I sought to study

fragmentation in multiple drums, which can be achieved by using a lithology with lower strength than the granodioritic rocks used by Arabnia and Sklar (2015).

The main objectives of this study are to 1) measure fragmentation probability and fragment size distribution with drop experiments; 2) to better understand how the particles size distribution evolves in rotating drums; 3) to create a numerical model code that explains how the particle size and mass evolves through travel distance; and 4) to explore the implications of laboratory experiments to particle fragmentation in the field. This research aims to achieve these main objectives and to create a framework that can tackle unanswered questions on fragmentation with different experiments and link them with a model. This work will ultimately help to understand the evolution of particle size distribution in debris flows and predict debris flow runout distance and the extent of debris flow hazards.

2.0 Experimental methods

2.1 Experimental design

To answer my research questions, I selected three rock types, granodiorite, serpentinite, and basalt (Figure 3). Granodiorite was used by Arabnia, 2015 because it is the lithology found in their field location at Inyo Creek, in the eastern escarpment of the southern Sierra Nevada mountains. In addition, I selected a lithology with a similar strength, basalt, and a weaker one, serpentinite. I wanted to test the idea that fragmentation rate scales with rock strength. I then ran serpentinite, the most breakable of the three rock types, in the rotating drums. I did not use basalt in the drum experiments because I wanted to contrast two rock types with significantly different strength.

Data from free-fall single-particle experiments and rotating drum experiments can be used to calibrate and test a numerical model that quantifies the production and size reduction of particles by fragmentation and abrasion in debris flows. These two methods used together allow me to explain fragmentation processes on different scales with different physics complexity.

2.2 Free-fall single-particle experiments

I used free-fall single-particle experiments to estimate abrasion and fragmentation in geophysical granular flows with a modified version of the free-fall experiments done

by Le Bouteiller et al. (2010). I tested angular particles of basalt, granodiorite, and serpentinite. I collected the basalt and serpentinite from different locations and used granodiorite already collected by Omid Arabnia and assistants. Basalt is from Grizzly Peak in Berkeley, CA. This rock has a tensile strength of 7.48±0.55 MPa (Leonard Sklar, personal communication, February 2, 2017) (Jones et al., 1991). Granodiorite is from the Graniterock Quarry in Aromas, CA and has a tensile strength of 7.6 MPa (Arabnia, 2015; Galloway et al., 2001). Serpentinite is from Mount Tamalpais in Marin county, CA, and it has a tensile strength of 5.37±0.26 MPa (Leonard Sklar, personal communication, February 2, 2017) (Sloan et al., 2006) (Figure 4).

I selected particles for three weight classes of 20 g, 100 g, and 1000 g respectively. Because of the scarce availability of weight classes of 10 g, I decided to use weight classes of 20 g instead. My assistants and I dropped a total of 183 particles, of which 48 were basalt, 68 granodiorite, and 67 serpentinite. The different number of particles dropped is due to the fact that I wanted to have enough fragmentation events for each rock type, since each rock type fragments in a different way on impact. The total number of rock drops was 3,655, including 806 basalt, 1,766 granodiorite, and 1,083 serpentinite (Table 1). We dropped the particles from different heights (0.1 m, 0.3 m, 0.6 m, 1 m, 2 m, and 3 m) onto the concrete floor of the laboratory. I selected this range to get as close as possible to velocities that debris flows have in the field. The impact point was enclosed within a bucket with the bottom removed, to prevent fragments from being

lost. I measured the particle mass before and after each fragmentation event. After a fragmentation event, the original ('parent') rock was collected and weighed, along with all fragments ('daughter particles'). I also dropped 15 particles, 5 for each lithology, saturated with water to test for any difference in fragmentation rate between dry and saturated rocks (Table 2).

I tested the compressive strength of the floor concrete in areas where I dropped the rocks using a Schmidt hammer (Figure 5). This tool has an arbitrary scale, called 'rebound' number, which ranges from 10 to 100. Compressive strength is correlated with the rebound number. I tested the compressive strength at 3 different locations with 5 measurements each. After an analysis of variance, I determined that the compressive strength is statistically the same at the 3 locations. The mean value of compressive strength is 47.1 ± 0.8 N/mm^2.

I defined a fragmentation event as occurring when there is production of at least one particle greater than 2 mm in diameter along the intermediate axis. In particle analysis, there are three axes mutually perpendicular: the longest (a-axis), the intermediate (b axis), and the shortest (c axis). The 2 mm cutoff is based on the classification from Kuenen, (1956) and it is also the cutoff between gravel and fines such sand, silt, and clay. To separate particles greater than 2 mm from those less than 2 mm I used a sieve with 2 mm screen size. I further subdivided particles coming from

fragmentation events into greater than and less than 0.2 g. This was necessary because the scale I used has a precision of ±0.1 g. The fragmentation probability reported in section 3.1 is based on particles greater than 2 mm and greater than 0.2 g.

I choose different drop heights to compare the impact velocity to typical velocities in debris flows. For a free-falling point-like object with no frictional effects, the impact velocity can be described by the equation:

$$v = \sqrt{(2gh)} \qquad\qquad\qquad \text{eqn.3}$$

Where v is impact velocity [L/T], g is the acceleration of gravity [L/T^2], and h is the drop height [L]. I used $g = 9.8$ m/s^2. The impact velocity for the drops varies between 1.4 m/s and 7.7 m/s, which are within the range of typical values estimated for debris flows occurring in nature (Iverson, 1997).

2.3 Rotating drum experiments

The rotating drum experiments were performed at the Richmond Field Station, which is part of the University of California's Berkeley Global Campus at Richmond Bay. I also performed some experiments at San Francisco State University in the Hensill Hall room 112. At the Richmond Field Station, I had the opportunity to use 2 different drums: the 1.65 m diameter ('Dawdy') drum and the 0.56 m diameter ('Maytag') drum. I also used a rotating drum of 0.20 m diameter in the lab at Hensill 112 (the 'Barrel'). The

0.56 m drum has been used previously for studying bedrock erosion and debris flow rheology (Hsu et al., 2014, 2008; Kaitna et al., 2014; Schneider et al., 2011). The drums are designed with vanes perpendicular to the flow to avoid sliding of the material against the wall of the drum.

I conducted runs with the 'Dawdy' drum (1.65 m) using granodiorite in order to complete part of the work done by Arabnia (2015). In addition, I performed runs with the 'Maytag' (0.56 m) drum and the 'Barrel' drum (0.20 m) using serpentinite. I used serpentinite because I hypothesized that it would be weaker than granodiorite based on the tensile strength. The drums are used to study the evolution of PSDs as a function of travel distance and drum diameter (Arabnia, 2015). All these experiments were done following the same procedure used by Arabnia (2015), in order to compare the behavior of two lithologies with different properties such as granodiorite and serpentinite. My assistants and I measured and weighed all the particles before running them in the drums. I loaded the 'Dawdy' drum (1.65 m) with ~100 kg of granodiorite particles, the 'Maytag' drum (0.56 m) with ~5 kg of serpentinite particles, and the 'Barrel' drum (0.2 m) with 174 g of serpentinite particles. After loading the particles in the drums, I poured water in them to reach up to the central rim. After the runs were done, I removed the bigger particles by hand, and the fines and water by wet-dry vacuum. My assistants and I weighed the particles using balances with precision of 0.1 g for the 'Dawdy' (1.65 m) and the 'Maytag' (0.56 m) drums, and a balance with precision 0.0001 g for the 'Barrel' drum

(0.2 m). We measured the three particle axes for the 'Dawdy' drum (1.65 m) with calipers. I used a sieve shaker for particle sizing to measure the particle size distribution of smaller particles.

For the granodiorite, I ran the 'Dawdy' drum (1.65 m) for a total tangential travel distance of 8 km (adding to Arabnia's runs) and measured the sediments and water with particles in suspension at 2 km, 4 km, and 8 km. I measured the a, b, and c axes with calipers, and the weight of all particles with b-axis > 8mm. I sieved all the smaller particles.

For the serpentinite, I ran both 'Maytag' (0.56 m) and 'Barrel' drums (0.2 m) for a cumulative distance of 1 km. I weighed all the particles greater than 0.2 g and sieved the smaller particles every 250 m for the 'Maytag' drum (0.56 m). For the 'Barrel' drum (0.2 m). I weighed all the particles before the run and after 1 km. I also stopped every 250 m and counted the particles above 2 mm, and between 0.710 mm and 2 mm.

To compare energy expenditure across drums, I used unit drum power, which is calculated as:

$$\frac{\Omega}{A} = \frac{\rho_b r u_t g S}{12} \qquad\qquad \text{eqn.4}$$

where Ω is power [ML^2/T^3], A is unit bed area [L^2], ρ_b is bulk density [M/L^3], u_t is tangential velocity [L/T], and S if flow surface slope [L/L]. The values for these parameters come from (Arabnia et al., 2015a).

3.0 Experimental Results

3.1 Fragmentation probability

A particle dropped against the concrete loses fragments through both abrasion and fragmentation processes. Sometimes, the parent rock gets split in half from the impact, other times there is just a minimal production of small fragments. In some cases, there is no production of particles from the impact. The fashion of fracturing should be influenced by lithology, drop height, rock size, pre-existing fractures, and the particle angularity (Le Bouteiller et al., 2011; Le Bouteiller and Naaim, 2011).

To calculate fragmentation probability, I divided the number of fragmentation events by total number of drops for each rock class. A class is defined as a unique combination of rock type, particle mass, and drop height. (For example: Granodiorite, 20 g, 1 m, and Basalt, 100 g, 2 m). Even if the impact creates more than one fragment (> 2 mm) for a single drop, in the fragmentation probability calculation this is considered as one fragmentation event.

I plotted in log-log space the drop height versus the fragmentation probability (Figure 6a-b-c). I grouped the data points by lithology and rock size and fit power functions to them. I chose the power function because it shows a better R-squared value than other equations, such as linear or exponential. The probability of fragmentation can have all the possible numbers from 0, meaning no fragments at all, to 1, meaning 100%

chance of obtaining a fragment at any drop for that class. Figure 6 illustrates that with increasing drop height there is a higher fragmentation probability for any given lithology and rock size. Drops with 1000 g class size show a greater fragmentation probability than the other two class sizes.

I decided to analyze other predictors of fragmentation such as energy because the fashion of fragmentation depends on both mass and drop height. Furthermore, some of the R-squared values for the curves are particularly low (Table 3).

I plotted in log-log space the impact energy versus the fragmentation probability (Figure 7). I used the same fragmentation probability values used for Figure 6. I calculated the impact energy E using the equation:

$$E = mgh$$
eqn.5

Impact energy E is equal to the pre-drop mass m multiplied by the acceleration of gravity g, and the drop height h. I used the value of 9.81 m/s^2 for g.

The fragmentation probability P can be represented by a power equation with a coefficient a multiplied by impact energy E raised to the power b.

$$P = aE^b$$
eqn.6

where $P = 1.0$ for $E > E_{threshold}$.

Figure 7 illustrates the relation described by eqn.6. Increasing impact energy leads to higher fragmentation probability for all rock types. Serpentinite fragments more easily than basalt and granodiorite for higher impact energies. Granodiorite has the lowest fragmentation probability for impact energy. Granodiorite has a bigger fit exponent meaning that is more sensitive to change in impact rate, while basalt has a lower exponent and is relatively less sensitive to change in impact energy. Values of the regression parameters for each rock type are listed in Table 4.

I also performed a multiple regression analysis considering the fragmentation probability versus the explanatory variables rock mass and drop height, for the three rock types (Figure 8). I used a log-linear relationship in which the fragmentation probability P is equal to the coefficient a multiplied by the mass m raised to the exponent c, and the drop height h raised to the exponent d.

$$P = am^c h^d$$
eqn.7

Values of the best-fit parameters for each rock type are listed in Table 5. This three-parameter equation provides a better fit to the fragmentation probability for basalt, having a higher R-squared than the fit with eqn.6 (0.74 versus 0.66). For granodiorite, both eqn.6 and eqn.7 have the same R-squared (0.74). For serpentinite, eqn.6 shows a better fit with R-squared of 0.77 versus 0.64 for eqn.7.

I calculated the standard deviation and standard error for each fragmentation probability class (Table 6). From the analysis, the percentage error in some cases is about 15-20 %, while in other instances is over 100 %, meaning that there is considerable uncertainty when each rock class is considered separately.

3.2 Fragment size distribution

The parent distribution is coarser than the daughter distribution because of fragmentation events. Most of the products are coming from fragmentation that produces particles greater than 0.2 mm in diameter. Figure 9a-b-c shows the results using the method of Le Bouteiller, in which the ratio of the mass of the daughter products to the mass of parents, which is called z, is plotted on the x-axis and the normalized cumulative number on plotted on the y-axis. The normalized cumulative number is calculated in a series of steps. First, the z values for a specific class are sorted from smallest to biggest. Second, the biggest z gets the value 1 and the smallest z gets assigned the bigger value with an increment of 1 each z value within the class. Finally, the normalized cumulative number is calculated dividing the values from 1 up over the total number of z.

Smaller class sizes show higher values of z for higher cumulative numbers for all 3 rock types. Figure 10a-b-c shows how all the different classes can be collapsed onto a single trendline for each rock type that describes that fining of the particles. The trendline regressions from Figure 10 are the results I applied in the numerical code that I used to

simulate particle size reduction. Figure 11a-b-c illustrates that particle size reduction in free-fall single-particle experiments can also be described by a tempered Pareto distribution (Le Bouteiller et al., 2011). The following equation describes the tempered Pareto distribution:

$$B(z) = am^{-b}e^{cm}$$
<div align="right">eqn.8</div>

where *B(z)* is the normalized cumulative number, *a*, *b*, and *c* are fit parameters, and *m* is particle mass. The Pareto distribution is a reasonably good fit of the 1000 g class size (Figure 11). Class size 20 g and 100 g do not fit with the Pareto distribution for higher fragment mass, and this can be observed for all three rock types.

To test for an effect of saturation, I also did free-fall single particle experiments using 15 saturated particles, 5 for each rock type. Figure 12 a-b-c show that dry and wet fragments tend to follow a similar trend in the way they fracture, for all the three rock types. Figure 12 d-e-f shows that the values for dry and saturated particles can be explained by the same power fit.

3.3 Evolution of particle size in rotating drum experiments

Particle size distributions became finer over a 1 km travel distance for all the drum runs, because of fragmentation and abrasion processes. Figure 13 and 14 show the results from drum runs with serpentinite. I plotted the travel distance versus mass fraction greater than 2 mm for the 'Barrel' drum (0.2 m) (Figure 13) and greater than 2.8 mm for

the 'Maytag' drum (0.56 m) (Figure 13). The particles ran in the 'Barrel' drum (0.2 m)

shows a greater abrasion coefficient than the particles ran in the 'Maytag' drum (0.56 m)

(Figure 13). Figure 14 shows the cumulative number of particles created versus the travel

distance. The number of fragments in the 'Barrel' drum (0.2 m) increases exponentially

up to 0.5 km and then slows down considerably, while the number of particles created in

the 'Maytag' drum (0.56 m) increase steadily with no peaks. The number of fragments in

the 'Barrel' drum (0.2 m) decreases after 0.5 km because particles greater than 2 mm

have been degraded into fragments less than 2 mm.

Figure 15 represents a comparison between data collected using serpentinite and

data collected using granodiorite in the experiments. Abrasion rate scales with the drum

size for the experiments conducted with granodiorite. The bigger the drum, the higher the

abrasion rate. From the data collected, serpentinite does not follow that pattern. The flow

created in the 2 drums ('Barrel' drum (0.2 m) and 'Maytag' drum (0.56 m)) are different

and I provide an explanation in the section 6.1. Figure 16 shows that rock type and drum

size scale with the number of particles created over distance. Tougher lithology such as

granodiorite creates fewer particles than a more friable lithology such as serpentinite. The

runs done in the 'Maytag' drum (0.56 m) show a steady number of particles created

around 100 units. The runs in the 'Barrel' drum (0.2 m) with granodiorite shows a loss in

particles because of creation of fines. The runs in the 'Barrel' drum (0.2 m) with

serpentinite show an exponential increase in the number of particles up to 0.5 km with

more than 500 particles created, and then a decrease down to ~350 particles created after 1 km.

4.0 Numerical modeling

4.1 Model development

The purpose of the model is to simulate the production of sediment by fragmentation of an initial size distribution according to empirically-defined relationships between probability of fracture and impact energy and empirically defined daughter size distribution. I used a code written by Dr. Leonard Sklar and Dr. Clifford S. Riebe with the software program MATLAB. I used data from the free-fall single particle and drum experiments to generate output helpful to understand the processes of fragmentation and abrasion occurring in debris flows. The code works with a set of particles, each with a unique mass, and in each interval of possible fragmentation, every particle has a fragmentation probability which determines whether the particle fragments or not (Figure 10a-b-c). Each fragment has an energy that is the product of the impact velocity, a model parameter, and the particle mass. The fragmentation probability is calculated with eqn.6. If the particle fragments, a single daughter particle is created, the size of which is determined from the drop data fit to the z distribution (eqn.8). Figure 17 shows the regression that I used to find the pre-factor and exponent in the probability-energy relationship. The empirical fit to the data is explained by the equation

$$N_c = az^{-b} \qquad \text{eqn.9}$$

where N_c is the cumulative number of particles with z equal or less than z, normalized by the total number of particles, and a and b are fit parameters from the data. For the model, I want to predict the z for each fragment produced so I rearranged the equation to be

$$z = k_n N_c^{-a_n} \qquad \text{eqn.10}$$

where k_n and a_n are model parameters coming from regression parameters and

$$k_n = \left(\frac{1}{a}\right)^{-1/b} \qquad \text{eqn.11}$$

and

$$a_n = \frac{1}{b} \qquad \text{eqn.12}$$

The largest fragment size is constrained to be less than or equal to half the parent mass, so there is a maximum of $z = 0.5$, which means there is a N_c minimum N_{c_min}, that depends on the fit parameters k_n and a_n.

$$N_{c\_min} = \left(\frac{k_n}{z_{max}}\right)^{1/a_n} \qquad \text{eqn.13}$$

The way the model implements eqn. 9 is to generate a random number between N_{c_min} and 1 which is N_c, then solve for z. By knowing the parent mass M_p, I can calculate the daughter mass M_d as

$$M_d = zM_p \qquad \text{eqn.14}$$

The code has 17 parameters that can be modified based on different factors such as lithology and drum size. The two most important parameters are impact velocity and impact rate, which are fundamental to generating fragments because they directly affect the energy and frequency of the collisions. Density varies with lithology, and the alpha parameter, which controls the abrasion rate, depends on the drums size and the lithology of the rocks used in the drum experiments. To compare the model predictions with the measurements from the drum runs, the model calculates two performance metrics. The first, CompNumber, is the difference between the modeled and measured total number of particles greater than the cutoff size. The second, CompSieveAbs, is the sum of the absolute differences in the mass of sediment in each of the sieve size bins, between modeled and measured in the lab.

4.2 Model results

I ran the model initially to show the result of a single run. I used dataset from my study and from Arabnia, 2015. The examples that I show here are Run 1 (250 m run) for the 'Big' drum (4 m) using granodiorite (Figure 18-19-20-21). Figure 18 shows how the probability density function (PDF) of particle masses changes before the run and after the run. The creation of a large number of small particles is noticeable in the left part of the red PDF. This is what I expect because it comes from the fragment distribution from drop experiments. To understand the sensitivity of the model to changes in the key parameters, impact rate and impact velocity, I plotted the mass versus the cumulative fraction for a

wide range of impact rate and impact velocities. The goal is to find a model output mass

size distribution that is as close as possible to the distribution measured after running

particles in the wheel. Figure 19 shows different combinations for low impact rate and

low impact velocity (Figure 19a), high impact rate low impact velocity (Figure 19b), low

impact rate high impact velocity (Figure 19c), and high impact rate high impact velocity

(Figure 19d). All these combinations are not good descriptors of particles after tumbling

drums. I then based my choice of optimal impact parameters on finding the value of

compNumber closest to 0 and the smallest compSieveAbs value. From Figure 20a, I can

see that optimizing compNumber results in representing the distribution of big fragments

accurately but smaller fragments and fines less well. On the other hand, Figure 20b shows

that optimizing compSieveAbs results in representing the fines accurately but the larger

fragments less well. To appreciate the range at which I have the optimum parameter

values Figure 21 shows contours lines of equal values for compNumber and

compSieveAbs. From Figure 22-23 I can appreciate that impact velocity and impact rate

values are scattered all over the graphs, not following specific trends over travel distance.

In Figure 22, I can see that the value of impact velocity and impact rate for the 'Maytag'

drum (0.56 m) with granodiorite are considerably higher than the impact rate and velocity

for the 'Maytag' drum (0.56 m) with serpentinite. I can observe a similar pattern in

Figure 23.

5.0 Field research

To understand my experimental and numerical results in the context of the field problem, I investigated the evolution of the size distribution of fine particles in a recent debris flow deposit. I hypothesize that energetic particle collisions in the debris flow should cause fragmentation and fining of the particle size distribution, which should be reflected in the size of fine sediments carried within the fluid part of the flow. I collected samples that can give information to explore this hypothesis.

5.1 Field site

Inyo Creek is a steep watershed draining part of the eastern Sierra Nevada close to Lone Pine, CA (Figure 24). The channel from the head down to the apex of the fan is approximately 3-km long with a total relief of 1,905 m, a contributing area of 3.1 km^2, and no evidence of Pleistocene glaciation (Brocklehurst and Whipple, 2004). Inyo Creek flows on nearly uniform lithology of granodiorites composed of the Whitney, Paradise, and Lone Pine plutons (Stone et al., 2000). The steepness of the slopes in the catchment allows frequent debris flows and rock avalanches. In July 15, 2013, a large debris flow occurred at Inyo Creek making this area a good field site for applying the insights from laboratory experiments.

5.2 Slack water samples

I collected samples of fine particles within debris flow deposits that I assigned the name "slack water". These fines are usually trapped between branches of trees torn down by the violence of debris flows. I also collected slack water samples higher up in the watershed between boulders. The collection was done at 11 locations between 1800 m and 3000 m of elevation to test for fining downstream of these deposits (Figure 25). Before collecting the particles, I scraped off the surface of approximately 2-3 cm that, because of rain and wind, started to form an armoring with coarser fines on the surface and finer particles beneath them (Figure 26). The samples were prepared by getting rid of the organic material and then sieved to assess the PSD of each location. Before sieving the particles, I dried them in oven for 24 hours at 120 degrees Celsius to eliminate any residual water content. I sieved the particles using a sieve shaker for particle sizing. I assembled a sieve stack with screen from phi 2.5 to phi -4. The higher up sieve screens are 1 phi size apart, same as for the 2 bottom ones. The other screen sieves are 0.5 phi size apart. I run the sieve shaker with the 'slack water' particles for a total of 6 minutes each sample analyzed.

5.3 Field results

The data from the sieved slack water samples show evidence of particle fining downstream. Figure 27 illustrates the particle size distribution of the samples collected

and we can infer that on average the D50 is decreasing with longer travel distance. Figure 28 suggests that particle size is decreasing with travel distance for the D16, D50, and D84 quantiles. An exponential equation represents this relationship

$$D = re^{-sx}$$ eqn.16

where D is the particle size [L], r and s are fit parameters and x is the travel distance [L]. These results are statistically significant, with calculated p-values of less than 0.01.

6.0 Discussion

6.1 Summary of significant findings

With higher drop height, the fragmentation probability increases for all the rock types taken in consideration for this study. Impact energy is a better predictor of fragmentation probability because it considers both the drop height and the mass of the particle dropped. Rocks with similar strength such as granodiorite and basalt do not have the same fragmentation probability, this leads me to think that there are other more important predictors. One of the predictors for fragmentation probability might be the fracture toughness. Fracture toughness is a property that describes the ability of a material containing a crack to resist fracture. Each rock type's fragment size distribution can be summarized by using a negative regression. Dry and saturated particles show similar fragmentation probability (Figure 12), so it is reasonable to use results from dry rocks in

the model even though some experimental and theoretical studies report a weakening of the material with saturation (Le Bouteiller et al., 2010).

Figure 13 illustrates results that I was not expecting. From the data, the 'Barrel' drum (0.2 m) produces a higher abrasion rate than the 'Maytag' drum (0.56 m). From my observations, I noticed that the flow in the 'Maytag' drum (0.56 m) and 'Barrel' drum (0.2 m) are visually very different. The 'Maytag' drum (0.56 m) shows a typical debris flow angle with water and sediments running together, while in the 'Barrel' drum (0.2 m) the water rests at the bottom while particles are stuck in the perpendicular vanes and get dropped once they reach the higher point in the device. A lower drum power for the 'Barrel' drum (0.2 m) should lead to a lower abrasion rate compared to the 'Maytag' drum (0.56 m) with a greater drum power. Figure 14 shows again unexpected results with a far greater number of particles created for the 'Barrel' drum (0.2 m) compared to the 'Maytag' drum (0.56 m). I do not believe that the difference in the cutoff for the two drums (>2 mm for 'Barrel' drum (0.2 m) and >2.8 mm for 'Maytag' drum (0.56 m)) can affect the general trend. Looking at Figure 15, I observe that the abrasion rate is much higher for the experiments conducted with serpentinite in the 'Barrel' drum (0.2 m).

Figure 20 gives a clear explanation of the model flaws in not picturing completely both processes of fragmentation and abrasion depending on the comparison value

considered. The expectations for Figure 22-23 were to find a decreasing impact rate and impact velocity with travel distance, but the data do not show this trend.

Data from the field suggests that there is a fining trend downhill, however I cannot attribute fining solely to debris flow abrasion. Hillslope and fluvial degradation of the debris flow deposit affect the particle size distribution. This shows the importance of controlled and simplified laboratory experiments.

6.2 Scaling from the lab to the field

One of the main goals of my research is to expand on the findings of Arabnia and Sklar, 2016 and with those and my other findings precisely estimate particle wear rates in the field. Figure 29a shows that from the data collected by Arabnia, it is possible to predict the abrasion rate in the field. The data I collected during the drum experiments with serpentinite, if not supported by other data, do not allow me to extend the abrasion rate to the field because of an apparent inverse relation between drum power and new particles. Figure 29b also gives hints on the production of new particles. In this case, drum experiments with granodiorite show a pretty steady production of particles up to the Dawdy drum (1.65 m) and then a peak in production for the 'Big' drum (4 m). The data collected from the serpentinite experiments once again shows a trend not expected with less particles produced for the 'Maytag' drum (0.56 m). Figure 30a illustrates how the

impact velocity and impact rate increase linearly with drum power for the parameter compNumber. A similar behavior is seen in Figure 30b for the parameter compSieveAbs.

6.3 Recommendations for future work

More studies are needed to address weathering processes in debris flows, especially fragmentation. Future work in this field could include runs up to 1 km with serpentinite for the Dawdy drum (1.65 m) to have better constraints for the abrasion rate and number of particles created. It would be helpful to test another rock type such as basalt in drum experiments to evaluate different lithological environments that present debris flows. Even though basalt and granodiorite have a similar rock strength, they might have a different fracture toughness. The data from the drops can follow more closely a Pareto distribution having more data, so I suggest to have more drops especially for the 20 g and 100 g sizes. This should allow to evaluate if the Pareto distribution can describe particle size reduction in drop experiments. I also suggest a hybrid approach using rocks tumbled in the drum for drop experiments to possibly have a better representation of real world saturated particles from a debris flow. The model created with MATLAB needs improvements to show outputs as close as possible to what happens in the rotating drums and ultimately in nature. I suggest to implement the model using the fits from Figure 12 e-f. In addition, it would be beneficial to count for the

viscosity and in general the interaction between particle-particle and particle-water that can affect the fashion of the fragmentation and abrasion.

7.0 Conclusions

Particle size reduction in debris flows is influenced by rock strength, energy of transport, pore pressure inside the flow, and the type of wear. Particle wear occurs through abrasion and fragmentation processes. While abrasion may be modeled with the Sternberg model, there are unanswered questions on the controls of fragmentation and how to model it.

I used free-fall single-particle and rotating drum experiments to gather data to characterize fragmentation processes. I tested three rock types: basalt, granodiorite, and serpentinite. I considered these lithologies because of their different rock strength and vicinity of the sources to San Francisco. I used these data to calibrate a code that allows to simulate the production of sediment by fragmentation of an initial size distribution according to empirical relationships between fragmentation probability and impact rate and empirically defined daughter size distribution. I, also collected 'slack water' samples at Inyo Creek, that is a watershed in the Eastern Sierra Nevada of California.

I found surprising results, especially for rotating drum experiments and the model. The fragmentation probability increases for all the rock types with higher drop height and

higher energy. The fragment size distribution can be described with a power function

with a negative exponent. Dry and saturated rocks fracture in the same fashion and with

similar frequency, so it is safe to use dry particles for the drop experiments. The 'Barrel'

drum (0.2 m) produces a higher abrasion rate than the 'Maytag' drum (0.56 m) because

of the difference in the flow dynamics. The model created with MATLAB shows impact

velocity and impact rate increase with drum size. Overall, the model needs to be

improved to better represent fragmentation processes. Data from the field suggest that

there is a fining trend downhill but this result might be biased because of the hillslope and

fluvial degradation of debris flow deposits.

REFERENCES

Arabnia, O., 2015. Particle size reduction in debris flows: laboratory experiments compared to field data from Inyo Creek, CA. San Francisco State University, San Francisco.

Arabnia, O., Sklar, L.S., 2016. Experimental Study of Particle Size Reduction in Geophysical Granular Flows. Int. J. Eros. Control Eng. 9, 122–129.

Arabnia, O., Sklar, L.S., 2015. Experimental Study of Particle Size Reduction in Debris Flows. San Francisco State University, San Francisco.

Arabnia, O., Sklar, L.S., Bianchi, G., Mclaughlin, M., 2015a. Experimental Study of Particle Size Reduction in Geophysical Granular Flows.

Arabnia, O., Sklar, L.S., Mclaughlin, M., 2015b. Experimental study of particle size reduction in debris flows.

Arattano, M., Marchi, L., 2008. Systems and sensors for debris-flow monitoring and warning. Sensors 8, 2436–2452.

Bowman, E.T., Take, W.A., Rait, K.L., Hann, C., 2012. Physical models of rock avalanche spreading behaviour with dynamic fragmentation. Can. Geotech. J. 49, 460–476. doi:10.1139/t2012-007

Brocklehurst, S.H., Whipple, K.X., 2004. Hypsometry of glaciated landscapes. Earth Surf. Process. Landf. 29, 907–926. doi:10.1002/esp.1083

Galloway, J.P., Weathers, J., Frank, D., 2001. Consumer uses of industrial minerals in the San Francisco Bay area—Houses to interstates. Geol. Nat. Hist. San Franc. Bay Area Field-Trip Guideb. 173–178.

Highland, L., Johnson, M., 2014. Landslide Types and Processes (No. Fact Sheet 2004-3072). U.S. Geological Survey.

Hsu, L., Dietrich, W.E., Sklar, L.S., 2014. Mean and fluctuating basal forces generated by granular flows: Laboratory observations in a large vertically rotating drum. J. Geophys. Res. Earth Surf. 119, 1283–1309. doi:10.1002/2013JF003078

Hsu, L., Dietrich, W.E., Sklar, L.S., 2008. Experimental study of bedrock erosion by granular flows. J. Geophys. Res. 113. doi:10.1029/2007JF000778

Iverson, R.M., 1997. The Physics of Debris Flows. Rev. Geophys. 35, 245–296.

Iverson, R.M., Logan, M., LaHusen, R.G., Berti, M., 2010. The perfect debris flow? Aggregated results from 28 large-scale experiments. J. Geophys. Res. 115. doi:10.1029/2009JF001514

Jones, David L., and G. H. Curtis., 1991. "Guide to the geology of the Berkeley Hills, central Coast Ranges, California. "Geologic Excursions in Northern California: San Francisco to the Sierra Nevada, California Division of Mines and Geology Special Publication 109 (1991): 63-74.

Kaitna, R., Dietrich, W.E., Hsu, L., 2014. Surface slopes, velocity profiles and fluid

    pressure in coarse-grained debris flows saturated with water and mud. J. Fluid

    Mech. 741, 377–403. doi:10.1017/jfm.2013.675

Kuenen, P.H., 1956. Experimental abrasion of pebbles: 2. Rolling by current. J. Geol.

    336–368.

Le Bouteiller, C., Guironnet, C., Naaim, F., Mathys, N., 2010. Experimental study of

    marl fragmentation. Presented at the EPFL Doctoral Conference in Mechanics,

    Geophysical Research Abstracts, Lausanne, Switzerland, p. 4.

Le Bouteiller, C., Naaim, M., 2011. Aggregate breakage under dynamic loading. Granul.

    Matter 13, 385–393. doi:10.1007/s10035-010-0235-2

Le Bouteiller, C., Naaim-Bouvet, F., Mathys, N., Lavé, J., 2011. A new framework for

    modeling sediment fining during transport with fragmentation and abrasion. J.

    Geophys. Res. 116. doi:10.1029/2010JF001926

Montserrat, S., Tamburrino, A., Roche, O., Niño, Y., 2012. Pore fluid pressure diffusion

    in defluidizing granular columns: PRESSURE DIFFUSION IN GRANULAR

    COLUMNS. J. Geophys. Res. Earth Surf. 117, n/a-n/a.

    doi:10.1029/2011JF002164

Schneider, D., Kaitna, R., Dietrich, W.E., Hsu, L., Huggel, C., McArdell, B.W., 2011.

    Frictional behavior of granular gravel–ice mixtures in vertically rotating drum

experiments and implications for rock–ice avalanches. Cold Reg. Sci. Technol. 69, 70–90. doi:10.1016/j.coldregions.2011.07.001

Sloan, Doris, and John Karachewski.,2006 Geology of the San Francisco Bay Region. Berkeley: University of California Press.

Stone, P., George, C.D., James, G.M., George, I.S., 2000. Geologic Map of the Lone Pine 15' Quadrangle, Inyo County, California. Geologic Investigation Series Map I-2617.

TABLES

Table 1: Summary of drop experiments for dry rocks.

Rock Type	Drop height (m)	Rock size (g)	# Rocks	#Drops	Rock Type	Drop height (m)	Rock size (g)	# Rocks	#Drops
Basalt	0.1	100	4	406	Serpentinite	0.1	100	5	340
Basalt	0.1	1000	3	26	Serpentinite	0.1	1000	3	11
Basalt	0.3	100	100	131	Serpentinite	0.3	20	5	183
Basalt	0.3	1000	3	11	Serpentinite	0.3	100	3	290
Basalt	0.6	20	3	56	Serpentinite	0.6	20	8	60
Basalt	0.6	100	3	29	Serpentinite	0.6	100	5	22
Basalt	0.6	1000	3	9	Serpentinite	0.6	1000	3	9
Basalt	1	20	5	48	Serpentinite	1	20	5	28
Basalt	1	100	3	16	Serpentinite	1	100	10	65
Basalt	1	1000	3	9	Serpentinite	1	1000	3	9
Basalt	2	20	3	18	Serpentinite	2	20	5	37
Basalt	2	100	3	14	Serpentinite	2	100	3	3
Basalt	2	100	3	10	Serpentinite	2	1000	3	9
Basalt	3	20	3	12	Serpentinite	3	20	3	19
Basalt	3	100	3	11	Serpentinite	3	100	3	9
Granodiorite	0.1	1000	5	110					
Granodiorite	0.3	100	5	493					
Granodiorite	0.3	1000	5	33					
Granodiorite	0.6	100	5	180					
Granodiorite	0.6	1000	3	36					
Granodiorite	1	20	5	276					
Granodiorite	1	100	10	183					
Granodiorite	1	1000	5	27					
Granodiorite	2	20	6	54					
Granodiorite	2	100	5	65					
Granodiorite	2	1000	3	9					
Granodiorite	3	20	8	251					
Granodiorite	3	100	3	11					

Table 2: Summary of drop experiments for saturated rocks. All of them are part of 100 g size from 1 m.

	Basalt	Granodiorite	Serpentinite
#rocks	5	5	5
#drops	30	94	17
#frag>0.2g	11	11	10

Table 3: Fit parameters and R-squared values for the power equation fits for Figure 6.

Rock type	Mass (g)	Coefficient	Exponent	R-squared
Basalt	20.00	0.09	1.69	0.94
Basalt	100.00	0.18	0.84	0.80
Basalt	1000.00	0.36	0.57	0.23
Granodiorite	20.00	0.01	1.60	0.18
Granodiorite	100.00	0.07	1.37	0.83
Granodiorite	1000.00	0.48	1.10	0.99
Serpentinite	20.00	0.09	1.17	0.85
Serpentinite	100.00	0.23	1.34	0.88
Serpentinite	1000.00	0.36	0.57	0.23

Table 4: Values of the regression parameters for Figure 7.

Rock type	Coefficient	Exponent	R-squared
Basalt	0.22	0.66	0.66
Granodiorite	0.06	1.03	0.75
Serpentinite	0.26	0.69	0.77

Table 5: Values of the regression parameters for Figure 8.

Rock type	Coefficient	Exponent	R-squared
Basalt	0.46	0.79	0.74
Granodiorite	0.99	1.23	0.74
Serpertinite	0.4	1.05	0.64

Table 6: Data points for fragmentation probability with standard error and percentage of standard error on the fragmentation probability. These data are used for producing Figure 6-7-8.

Rock type	Drop Height (m)	Rock size (g)	Frag prob	SE	SE/Frag prob	Rock type	Drop Height (m)	Rock size (g)	Frag prob	SE	SE/Frag prob
Basalt	0.1	100	0.02	0.02	0.70	Granodiorite	1.0	1000	0.56	0.17	0.31
Basalt	0.1	1000	0.19	0.05	0.28	Granodiorite	2.0	20	0.20	0.12	0.57
Basalt	0.3	100	0.04	0.01	0.39	Granodiorite	2.0	100	0.15	0.07	0.43
Basalt	0.3	1000	0.36	0.22	0.61	Granodiorite	2.0	1000	0.89	0.11	0.13
Basalt	0.6	20		0.00		Granodiorite	3.0	20	0.01	0.02	1.41
Basalt	0.6	100	0.28	0.17	0.60	Granodiorite	3.0	100	0.20	0.15	0.76
Basalt	0.6	1000	0.67	1.46	2.19	Serpentinite	0.1	100	0.02	0.04	2.48
Basalt	1.0	20	0.08	0.06	0.73	Serpentinite	0.1	1000	0.18	0.10	0.55
Basalt	1.0	100	0.25	0.12	0.50	Serpentinite	0.3	20		0.00	
Basalt	1.0	1000	0.67	0.19	0.29	Serpentinite	0.3	100	0.04		0.00
Basalt	2.0	20	0.39	0.26	0.66	Serpentinite	0.6	20	0.04	0.03	0.87
Basalt	2.0	100	0.21	0.14	0.67	Serpentinite	0.6	100	0.04	0.06	1.73
Basalt	2.0	1000	0.70	0.15	0.21	Serpentinite	0.6	1000	0.04	0.22	6.06
Basalt	3.0	20	0.50	0.23	0.47	Serpentinite	1.0	20	0.14	0.08	0.54
Basalt	3.0	100	0.36	0.02	0.06	Serpentinite	1.0	100	0.30	0.09	0.32
Granodiorite	0.1	1000	0.04	0.03	0.80	Serpentinite	1.0	1000	0.78	0.22	0.29
Granodiorite	0.3	100	0.01	0.03	5.17	Serpentinite	2.0	20	0.24	0.09	0.38
Granodiorite	0.3	1000	0.12	0.06	0.45	Serpentinite	2.0	100	1.00	0.00	0.00
Granodiorite	0.6	100	0.06	0.02	0.35	Serpentinite	2.0	1000	1.00	0.00	0.00
Granodiorite	0.6	1000	0.31	0.05	0.17	Serpentinite	3.0	20	0.26	0.06	0.24
Granodiorite	1.0	20	0.00	0.00	0.50	Serpentinite	3.0	100	1.00	0.00	0.00
Granodiorite	1.0	100	0.13	0.03	0.27						

FIGURES
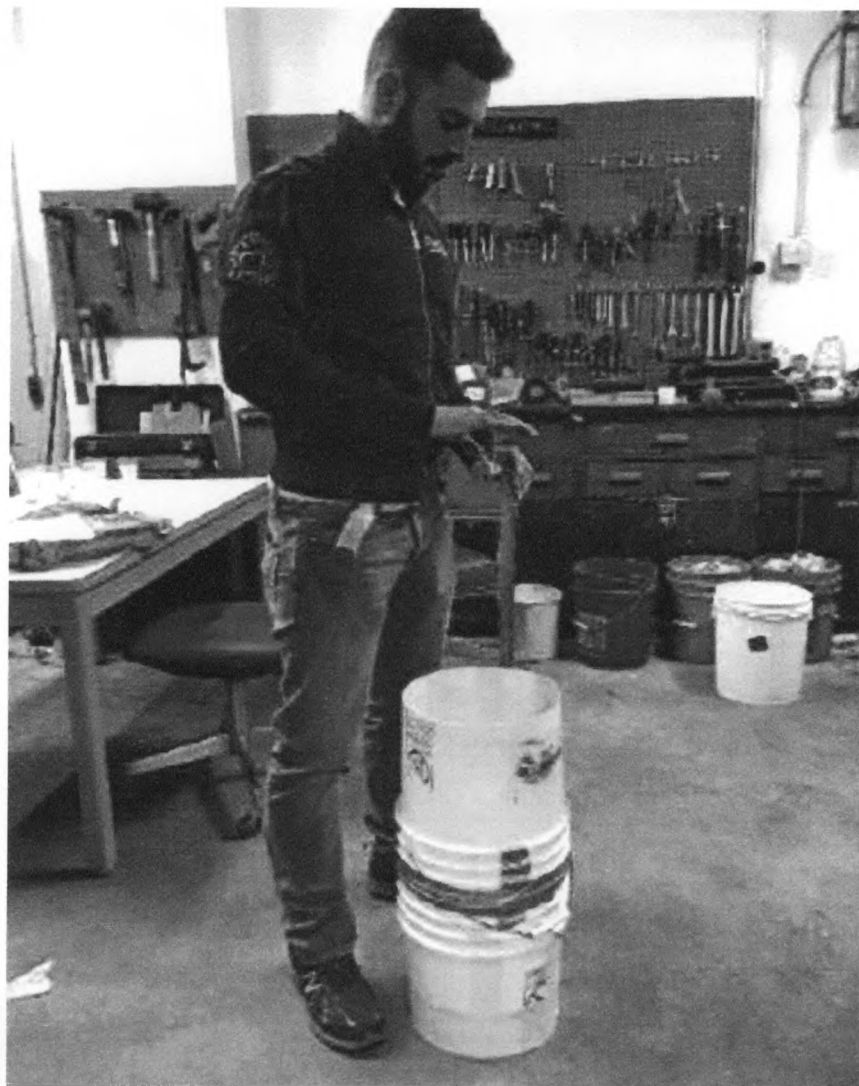
Figure 1: Example of a free-fall single-particle experiment from 1m at the Richmond Field Station. The bucket has no bottom to facilitate the impact against concrete and collect the fragments.
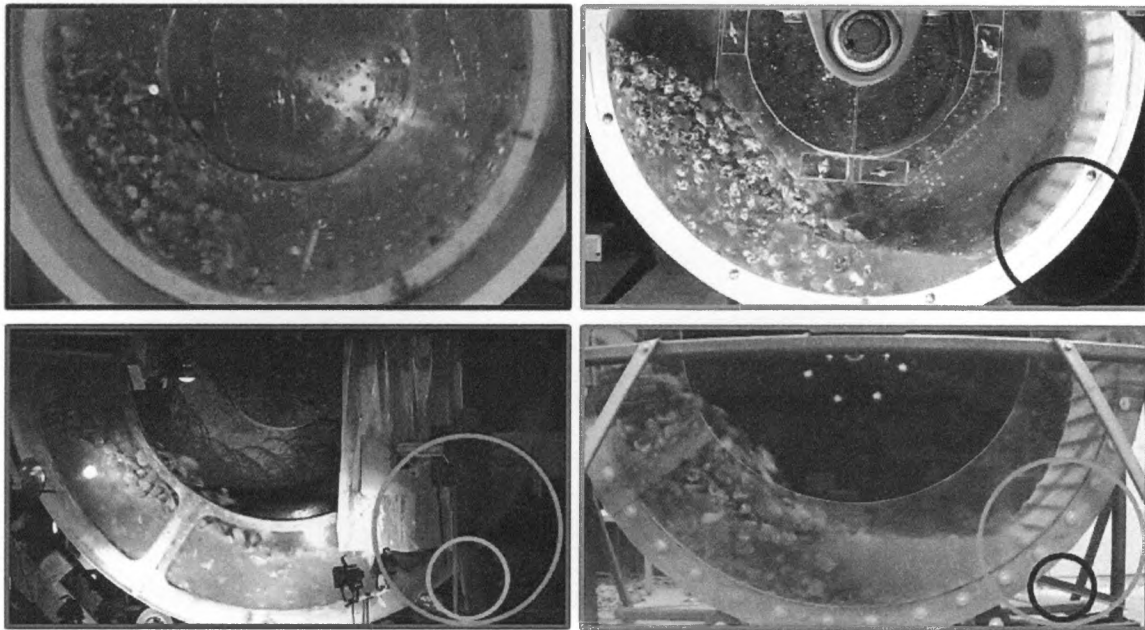
Figure 2: Rotating drums at the Richmond Field Station and Hensill 112. The drum in the blue rectangle (upper left corner) is the smallest (0.20 m diameter) and the drum in the red rectangle is the largest (4 m diameter) (lower left corner). The circles offer a way of comparing the drum diameters based on the color (figure from Arabnia et al., 2015b).

Figure 3: Rock types used in the free-fall single-particle and rotating drum experiments. From left to right: basalt, granodiorite, and serpentinite.

Figure 4: Google Earth Image with basalt, granodiorite, and serpentinite sites.

Figure 5: Measuring the compressive strength of one of the drop locations with the Schmidt hammer.
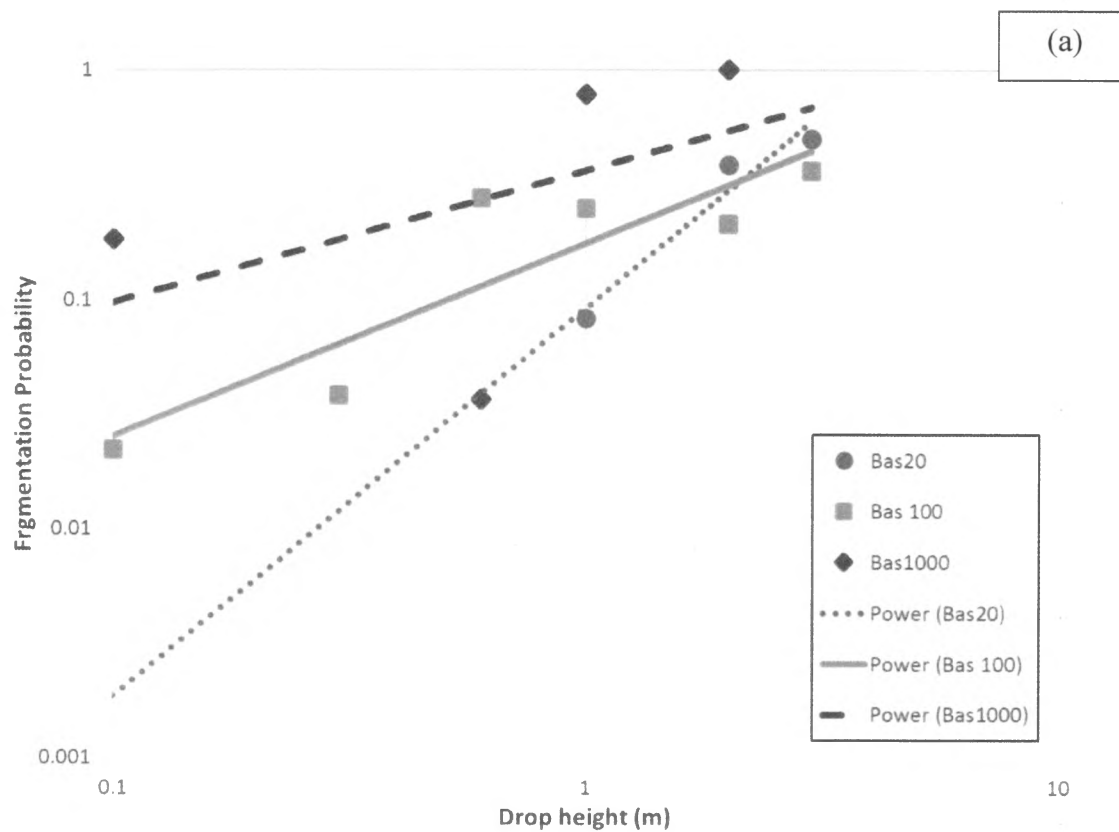
Figure 6a: Plot showing the relation between drop height and fragmentation probability for different particle mass classes, for basalt. Each point represents the average of the fragmentation probability for each class.
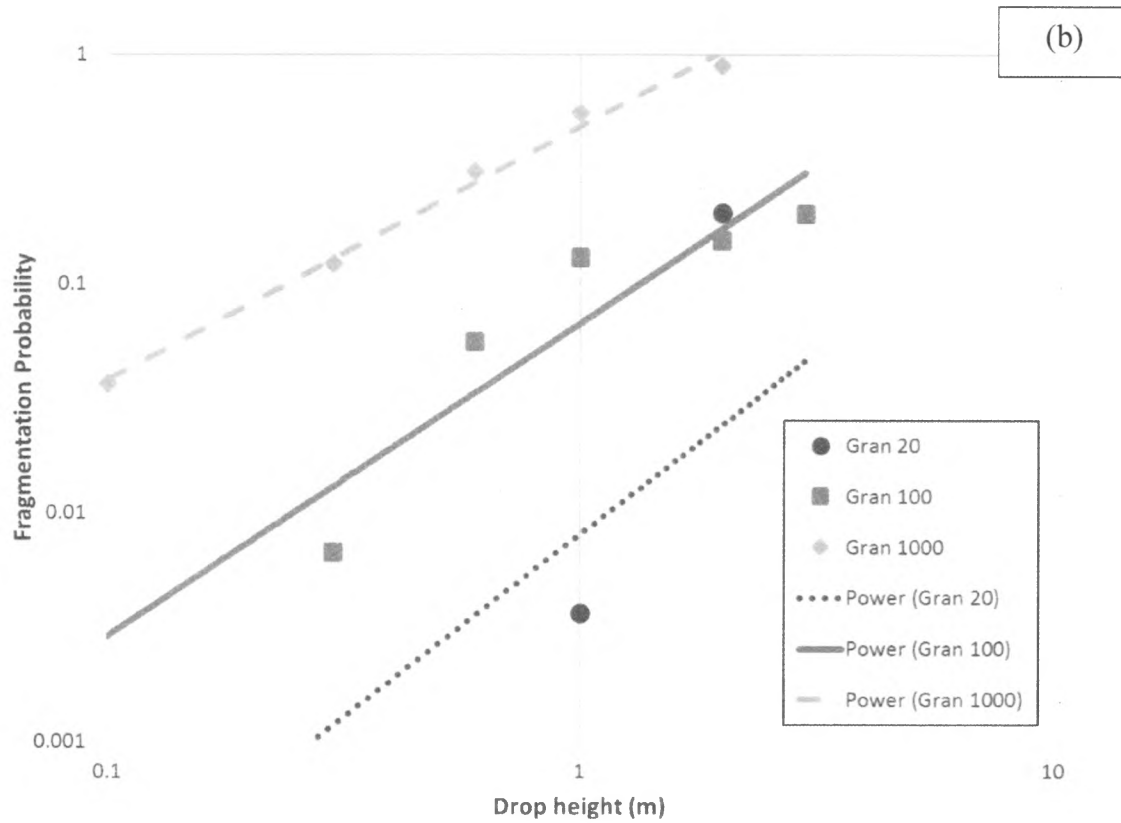
Figure 6b: Plot showing the relation between drop height and fragmentation probability for different particle mass classes, for granodiorite. Each point represents the average of the fragmentation probability for each class.
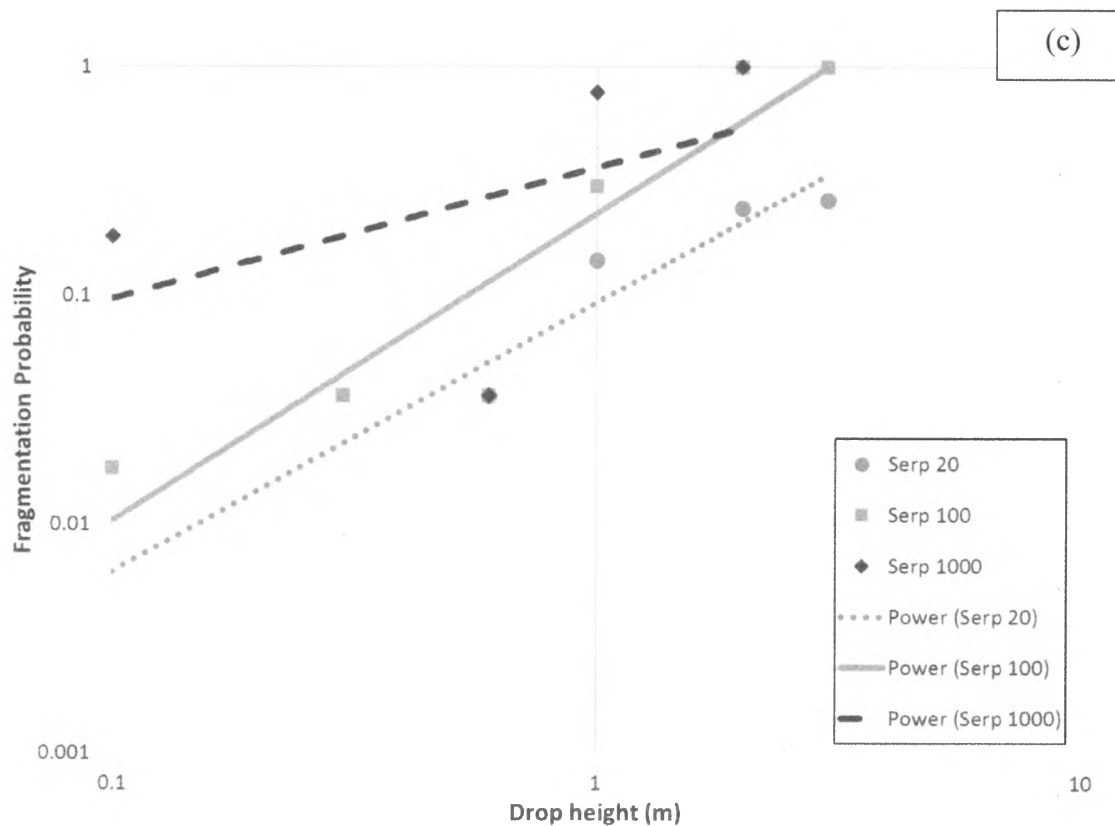
Figure 6c: Plot showing the relation between drop height and fragmentation probability for different particle mass classes, for serpentinite. Each point represents the average of the fragmentation probability for each class.
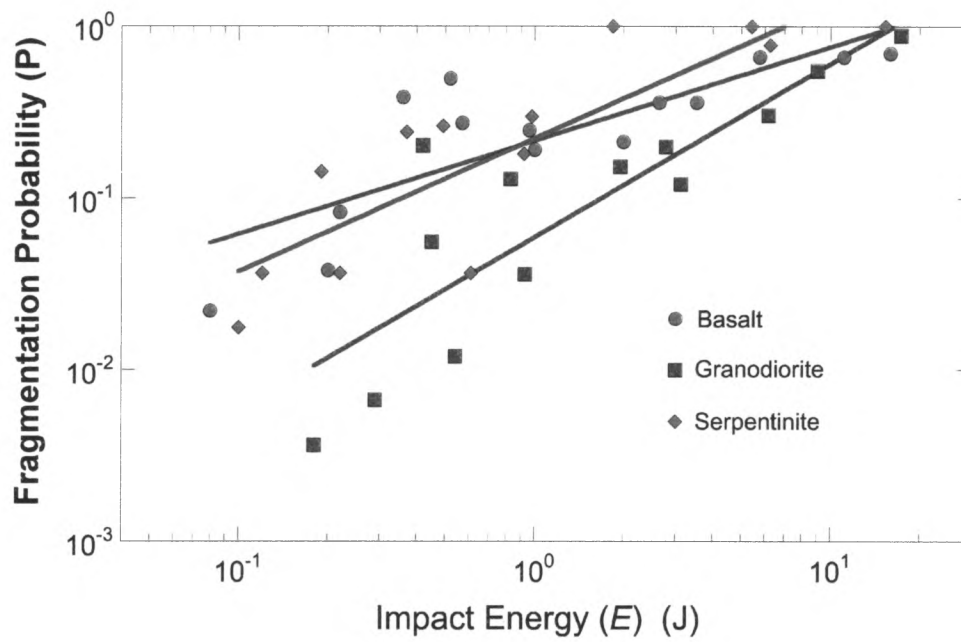
Figure 7: Plot showing the relationships between energy and fragmentation probability for basalt, granodiorite, and serpentinite.
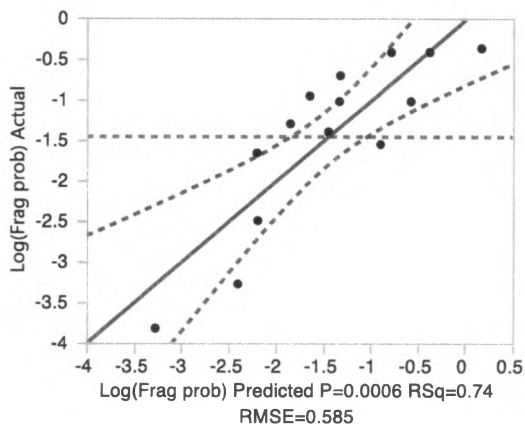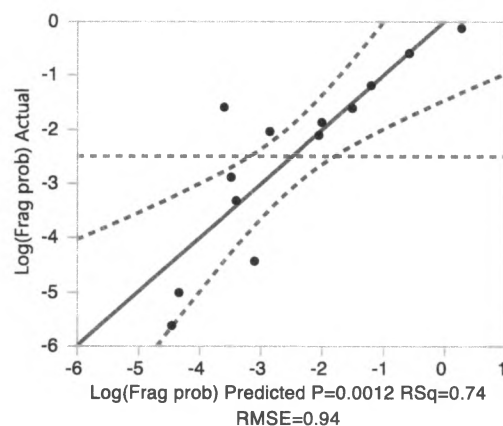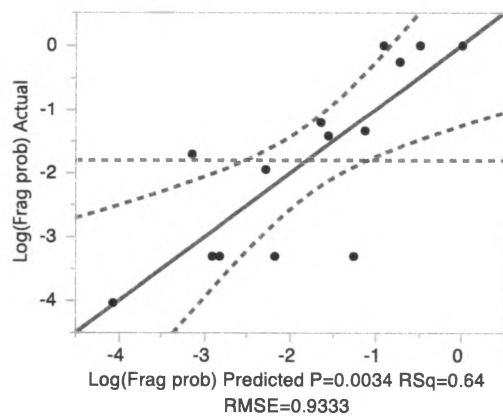
Figure 8: Actual by predicted plots of fragmentation probability as a function of both drop height and particle mass, from free-fall single-particle experiments for basalt (a), granodiorite (b), and serpentinite (c).

(a)
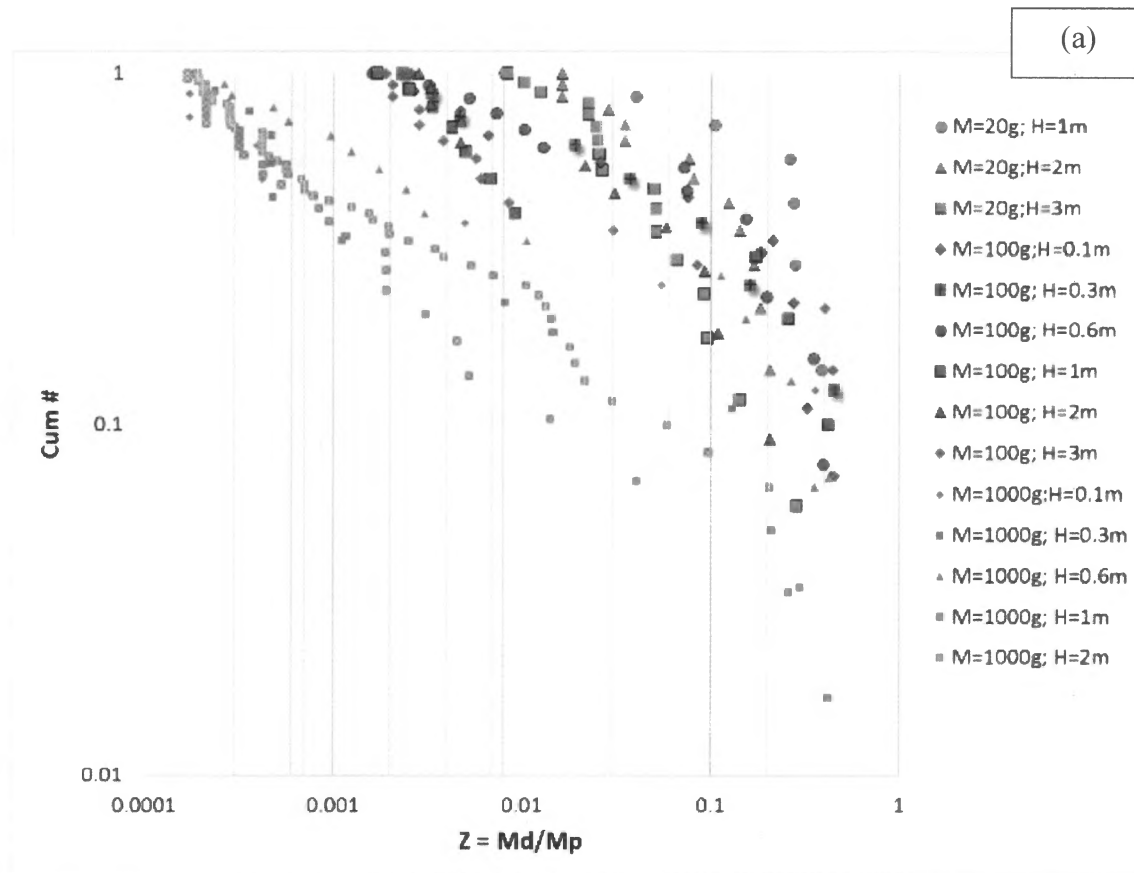
Figure 9a: Fragment size distribution normalized for basalt after Le Bouteiller et al., 2011. The y-axis shows the normalized cumulative number and x axis the ration between the mass of the daughter versus the mass of the parents.
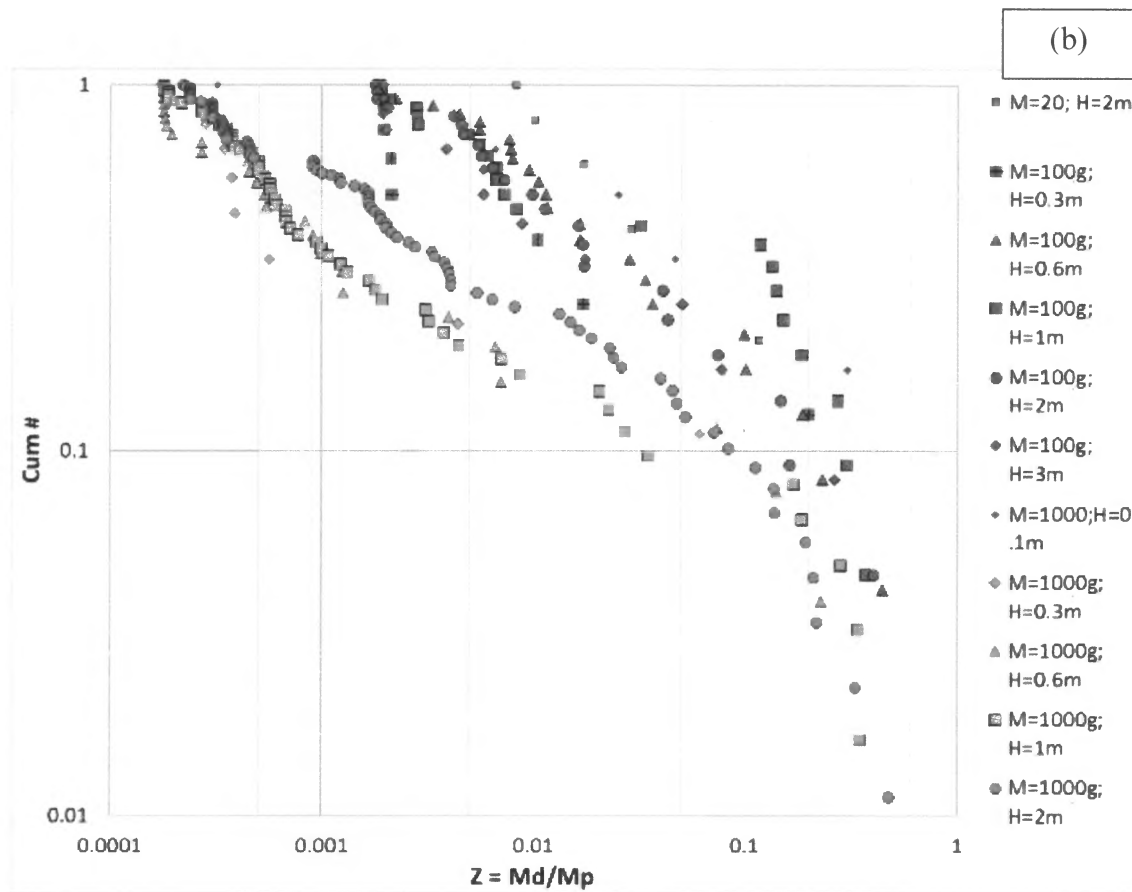
Figure 9b: Fragment size distribution normalized for granodiorite after Le Bouteiller et al., 2011. The y-axis shows the normalized cumulative number and x axis the ration between the mass of the daughter versus the mass of the parents.
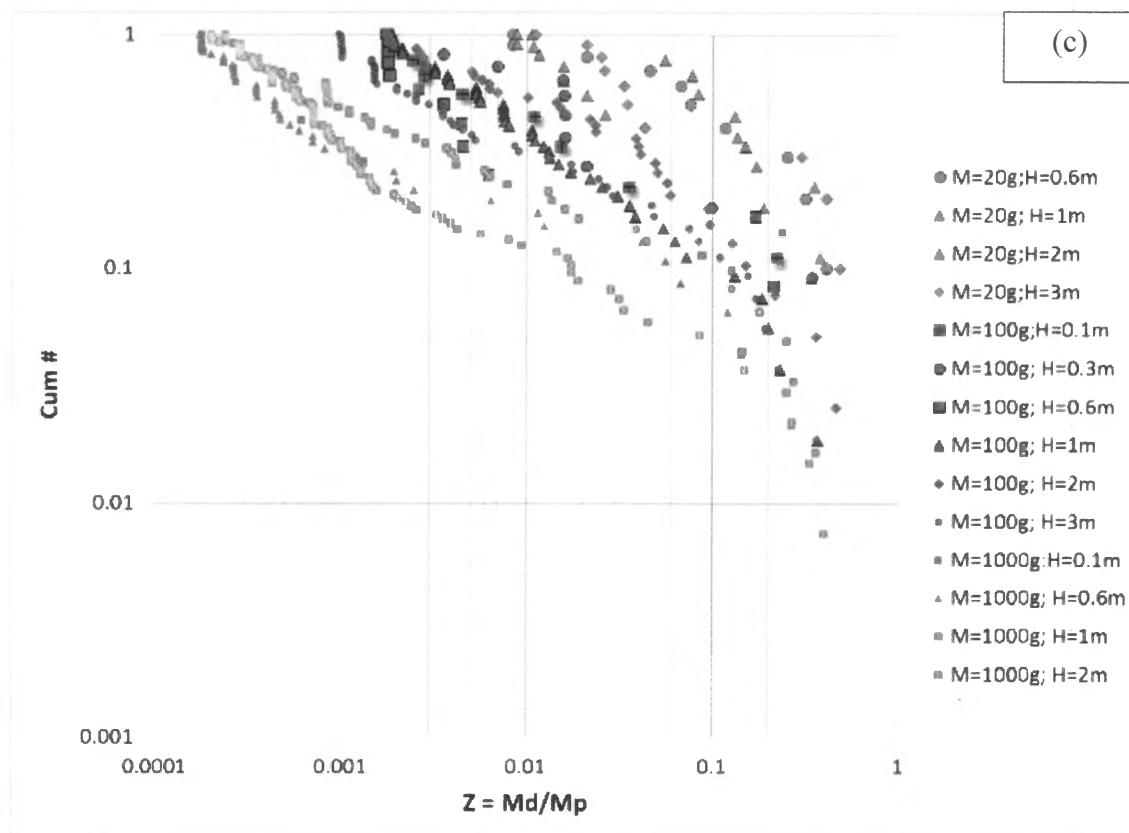
Figure 9c: Fragment size distribution normalized for serpentinite after Le Bouteiller et al., 2011. The y-axis shows the normalized cumulative number and x axis the ration between the mass of the daughter versus the mass of the parents.
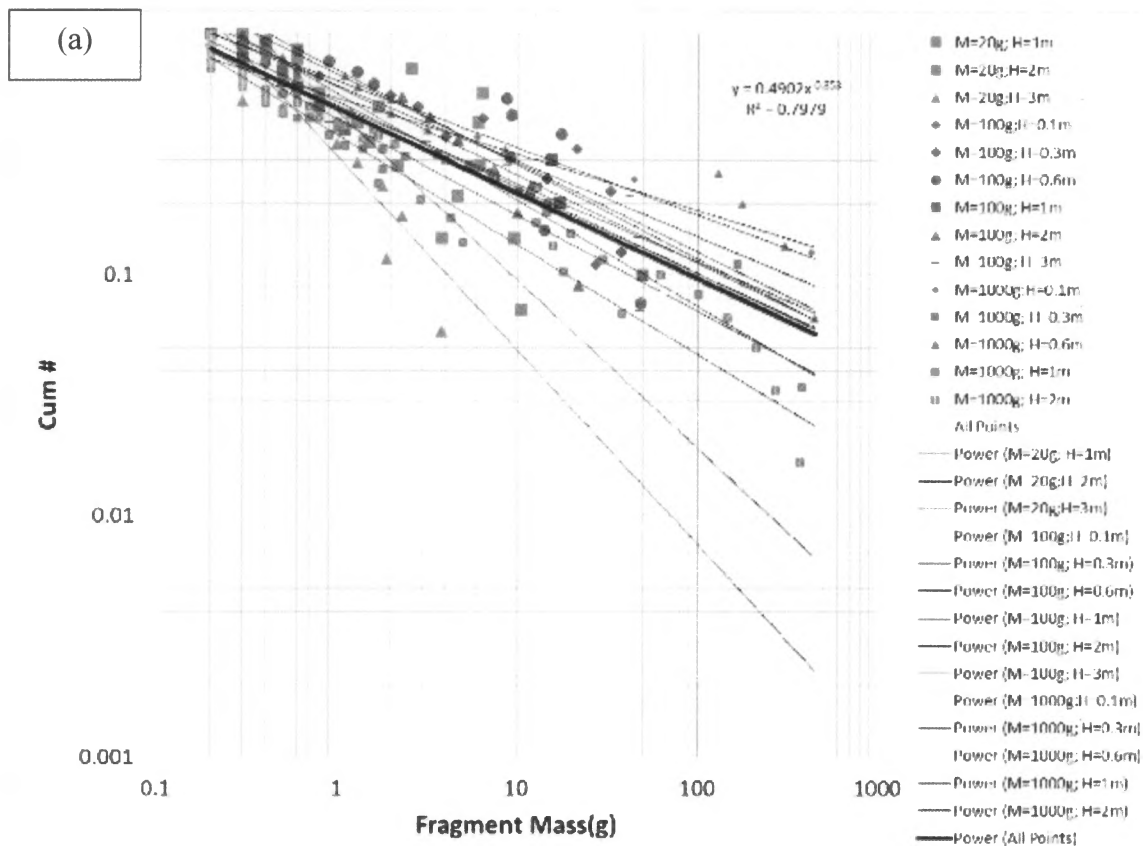
Figure 10a: Fragment size distribution for basalt. The regression and R-squared in the upper right corner are related power line using all points.
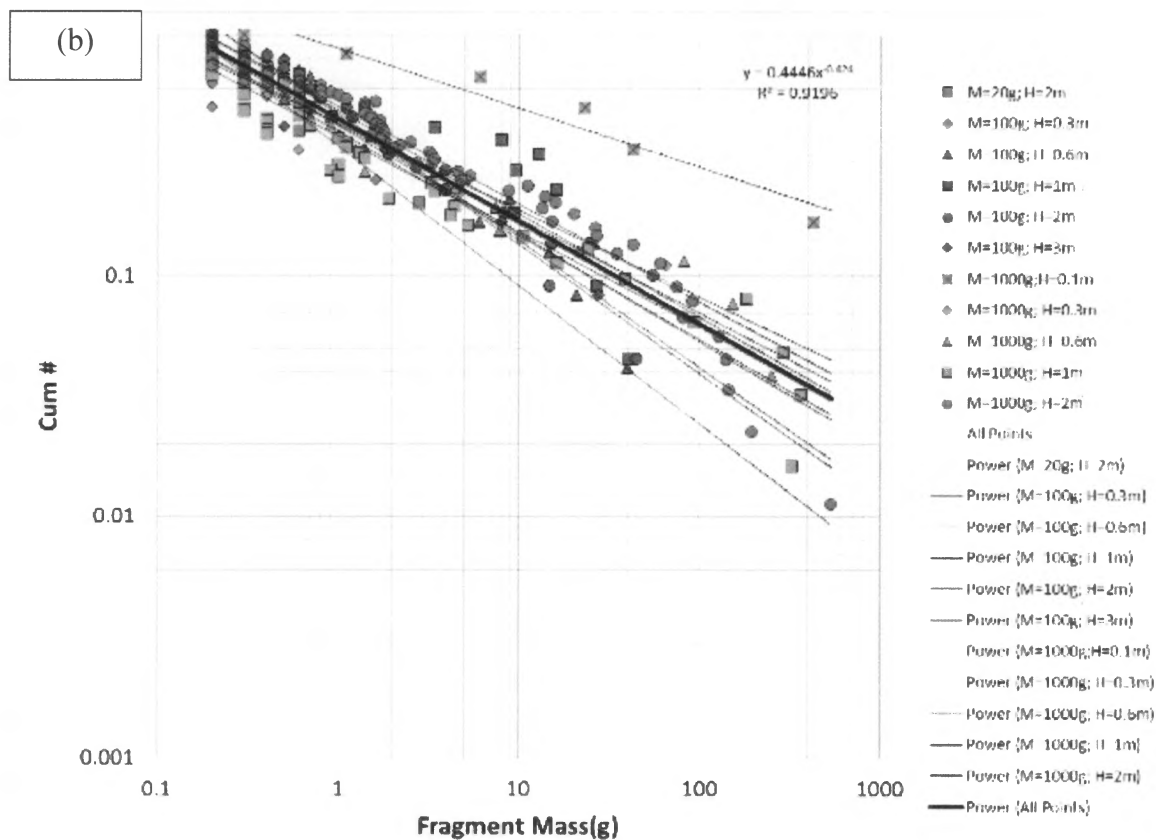
Figure 10b: Fragment size distribution for granodiorite. The regression and R-squared in the upper right corner are related power line using all points.
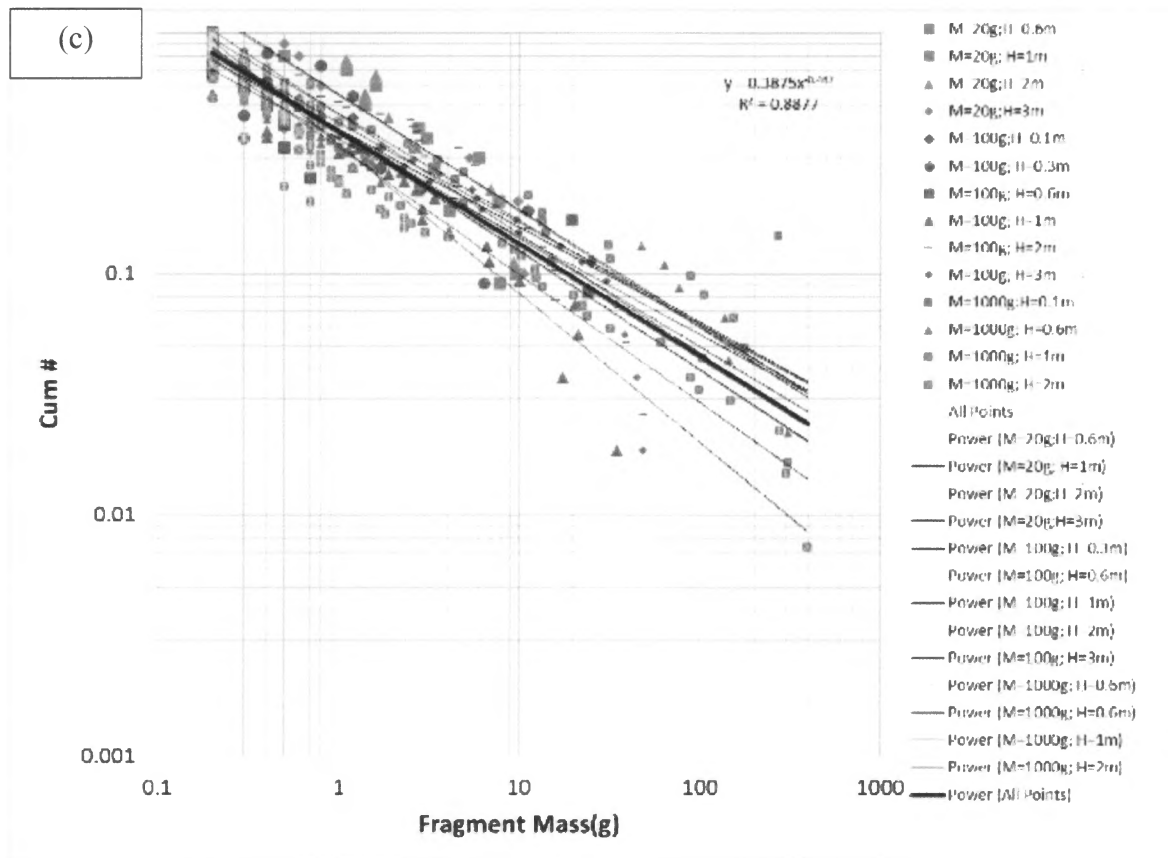
Figure 10c: Fragment size distribution for serpentinite. The regression and R-squared in the upper right corner are related power line using all points.
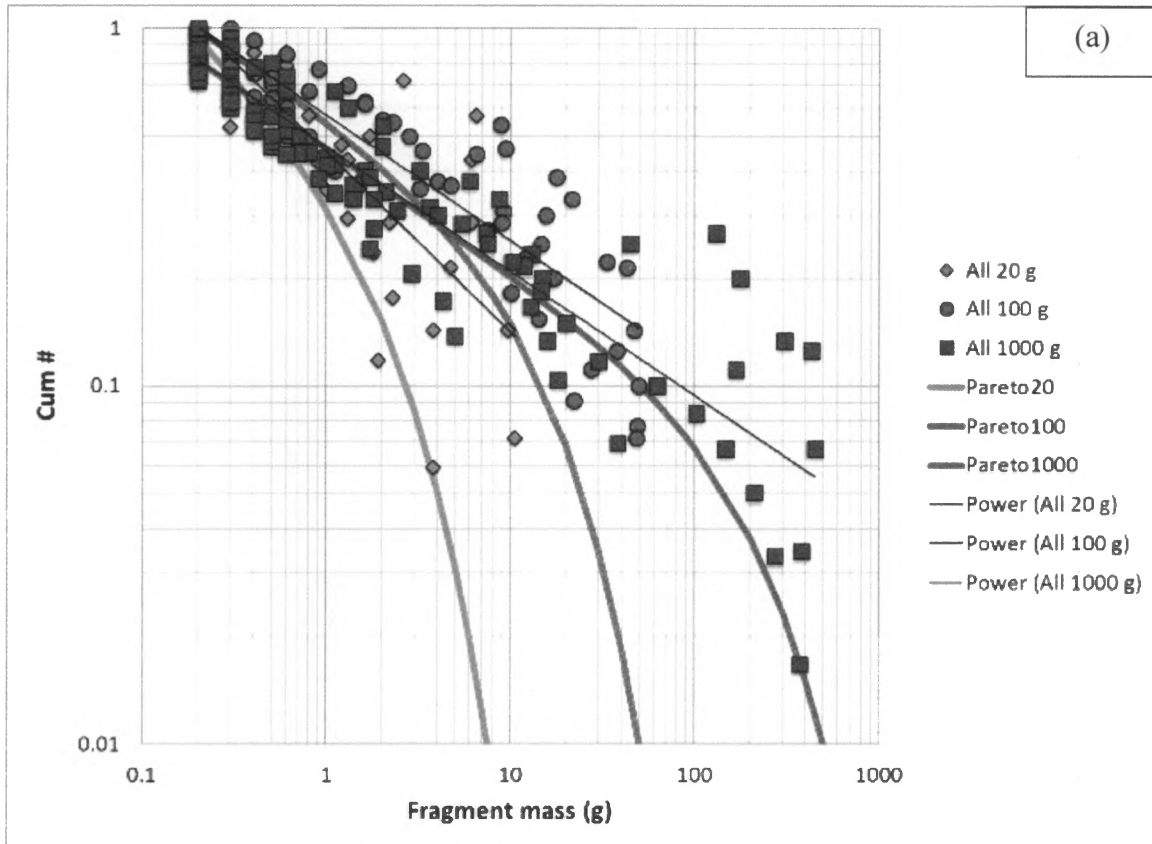
Figure 11a: Fragment size distribution from all heights combined for basalt and their tempered Pareto fits.
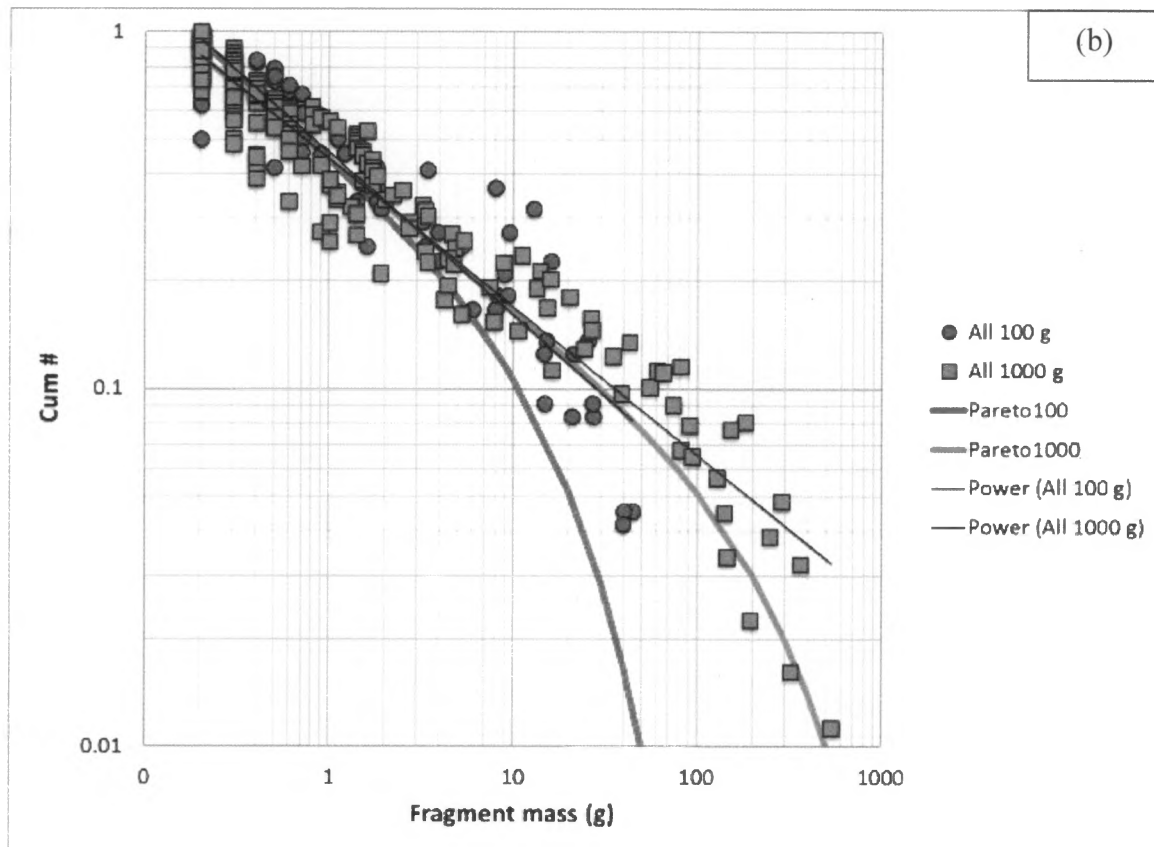
Figure 11b: Fragment size distribution from all heights combined for granodiorite their tempered Pareto fits.
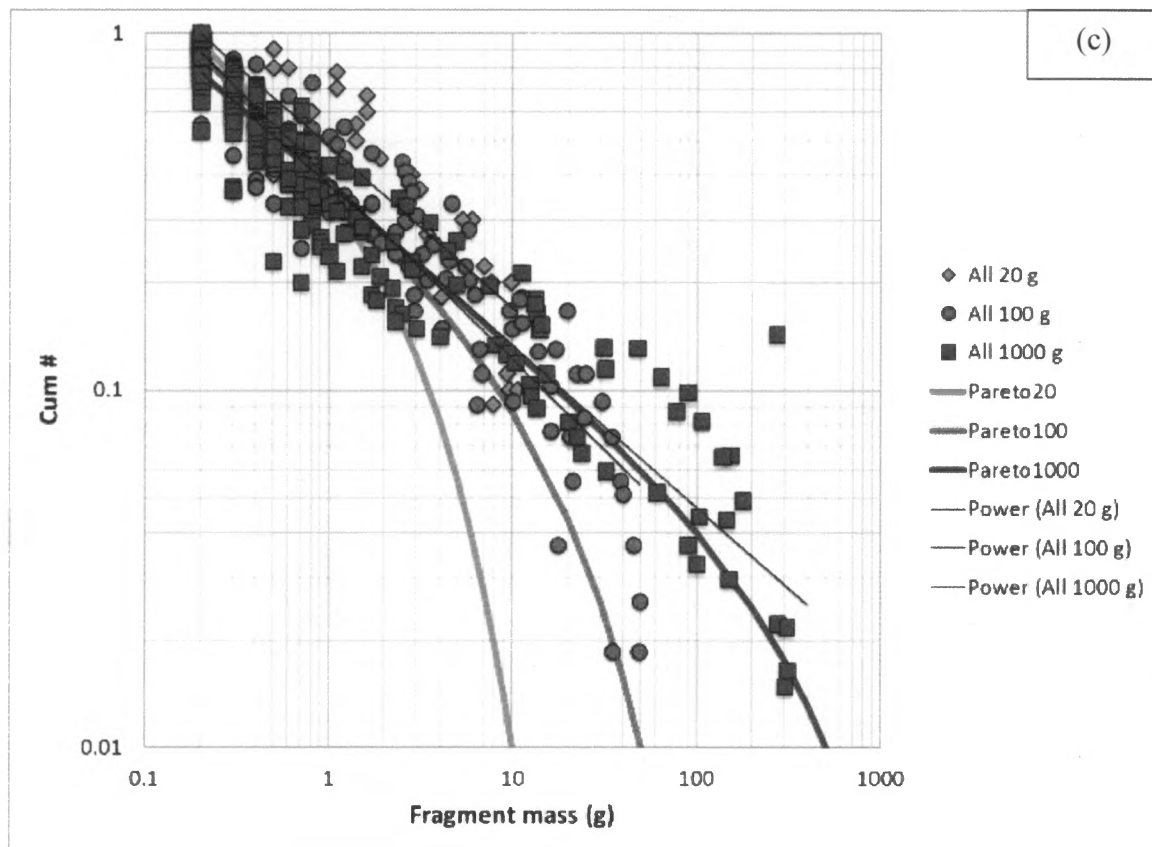
Figure 11c: Fragment size distribution from all heights combined serpentinite and their tempered Pareto fits.
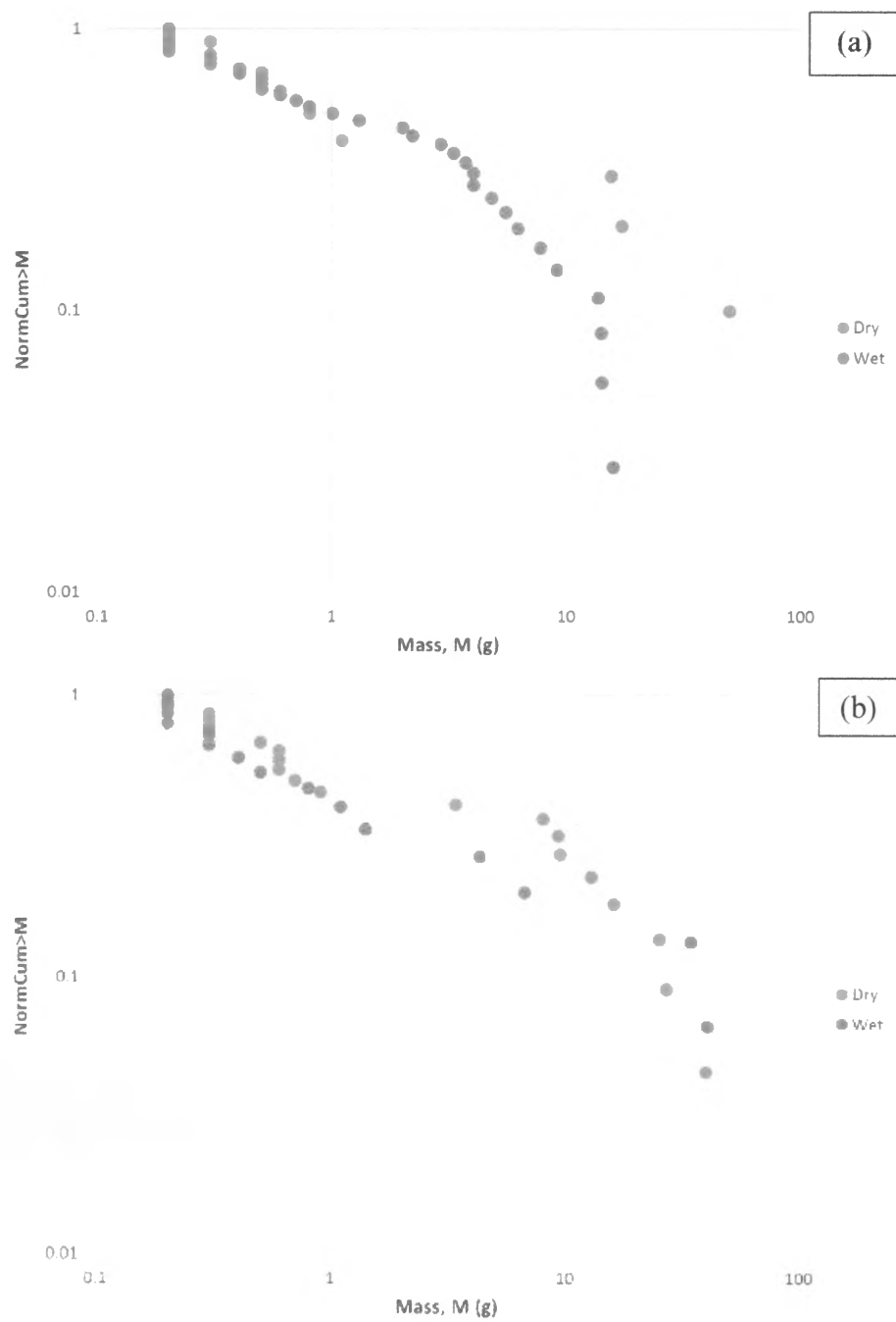
Figure 12: Mass versus Normcum>M for basalt (a) and granodiorite (b).
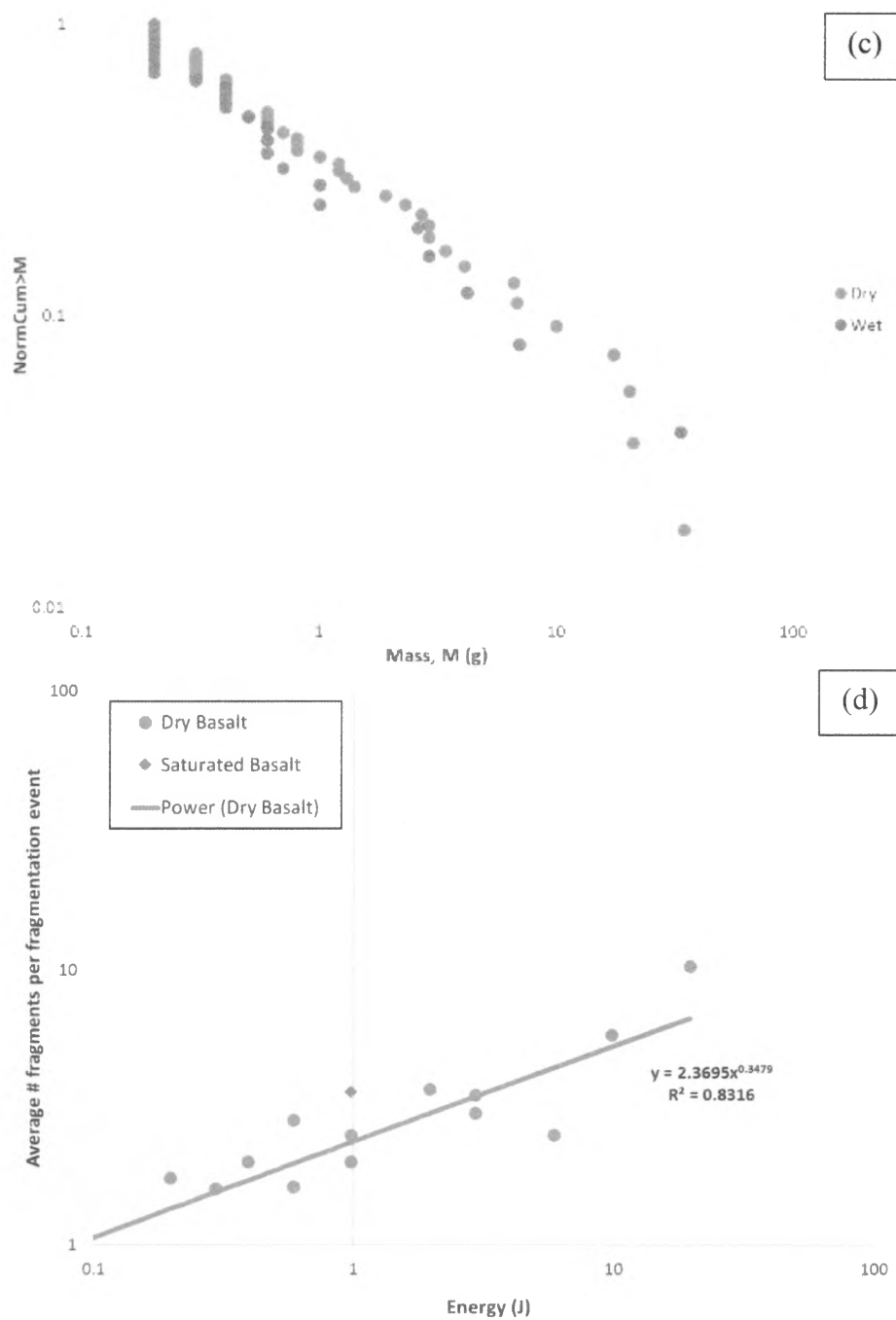
Figure 12: Mass versus Normcum>M serpentinite (c). Energy versus Frag>0.2 g for basalt (d).

(e)

(f)
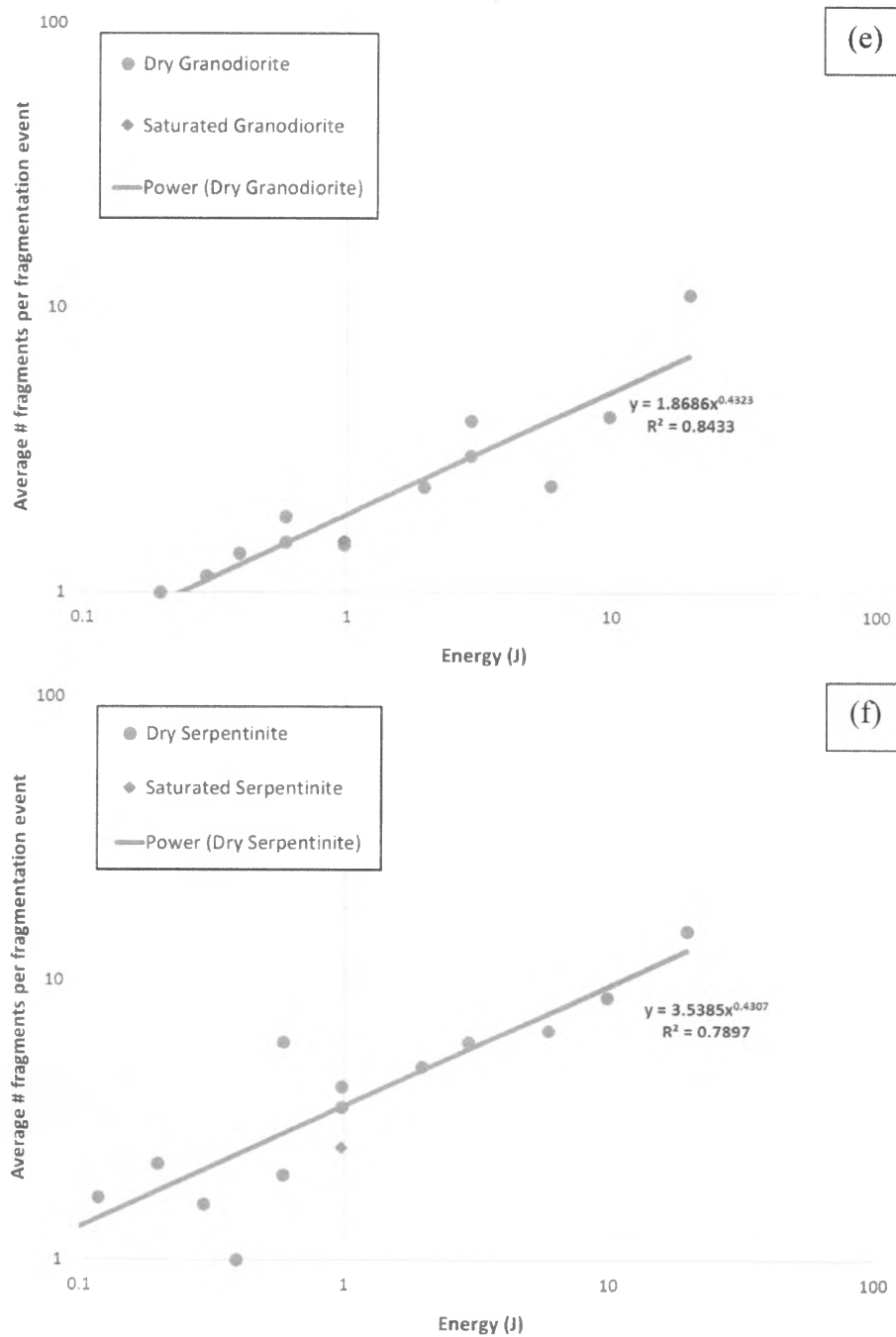
Figure 12: Energy versus Frag>0.2 g for granodiorite (e), and serpentinite (f).
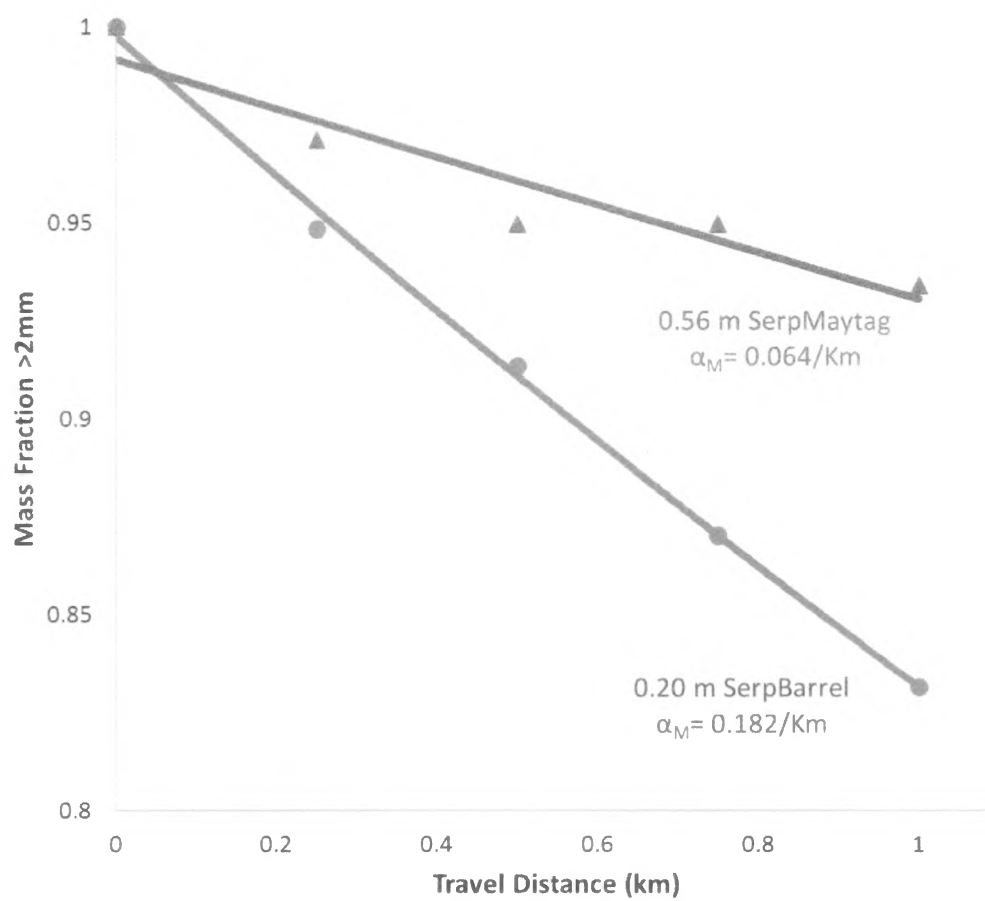
Figure 13: Mass loss from coarse size fraction.
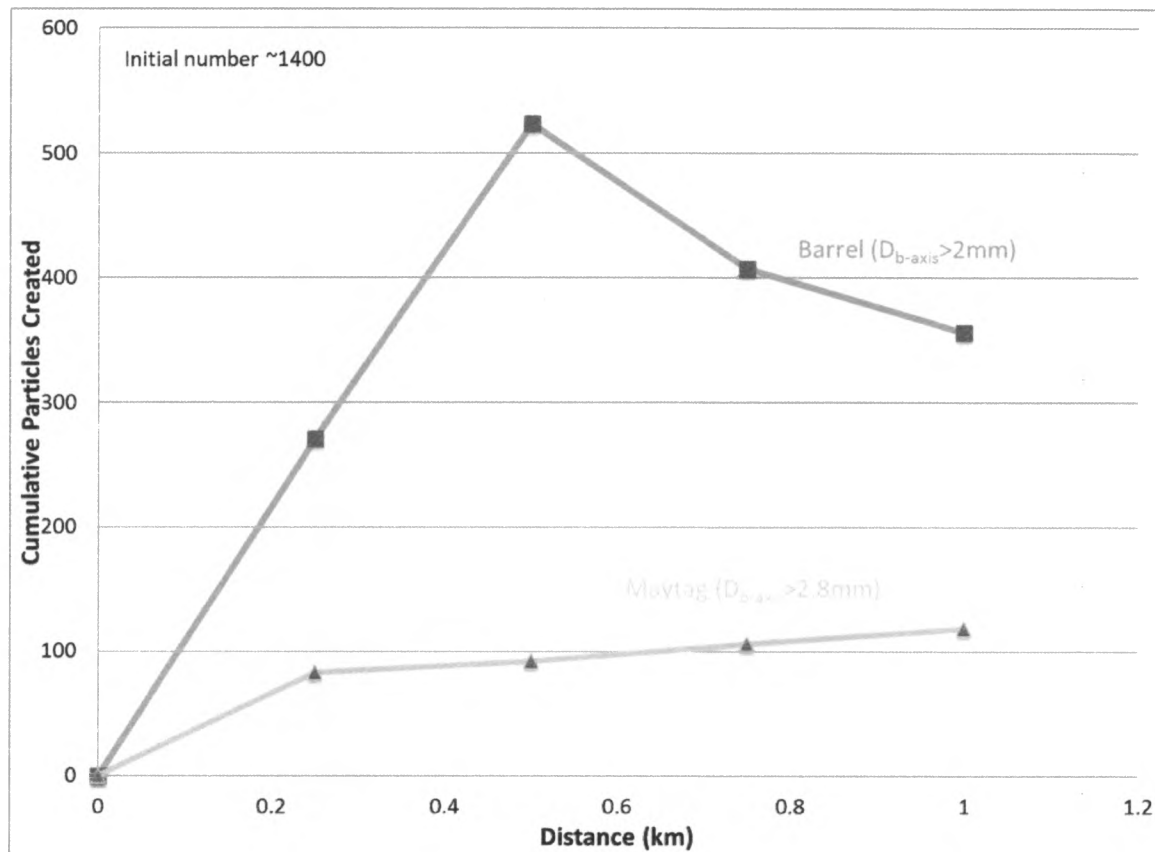
Figure 14: Number of particles created versus travel distance.
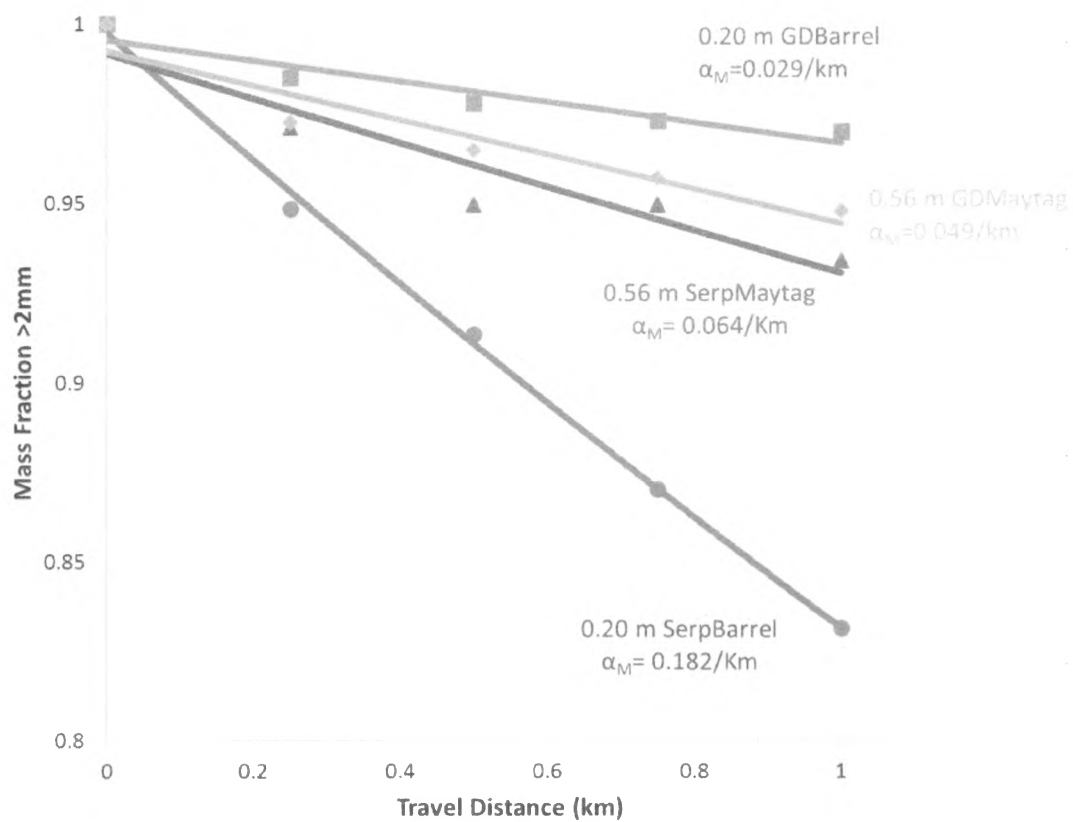
Figure 15:Comparison of abrasion rates from this study (Serp=serpentinite) with Arabnia and Sklar, 2016 (GD=Granodiorite).
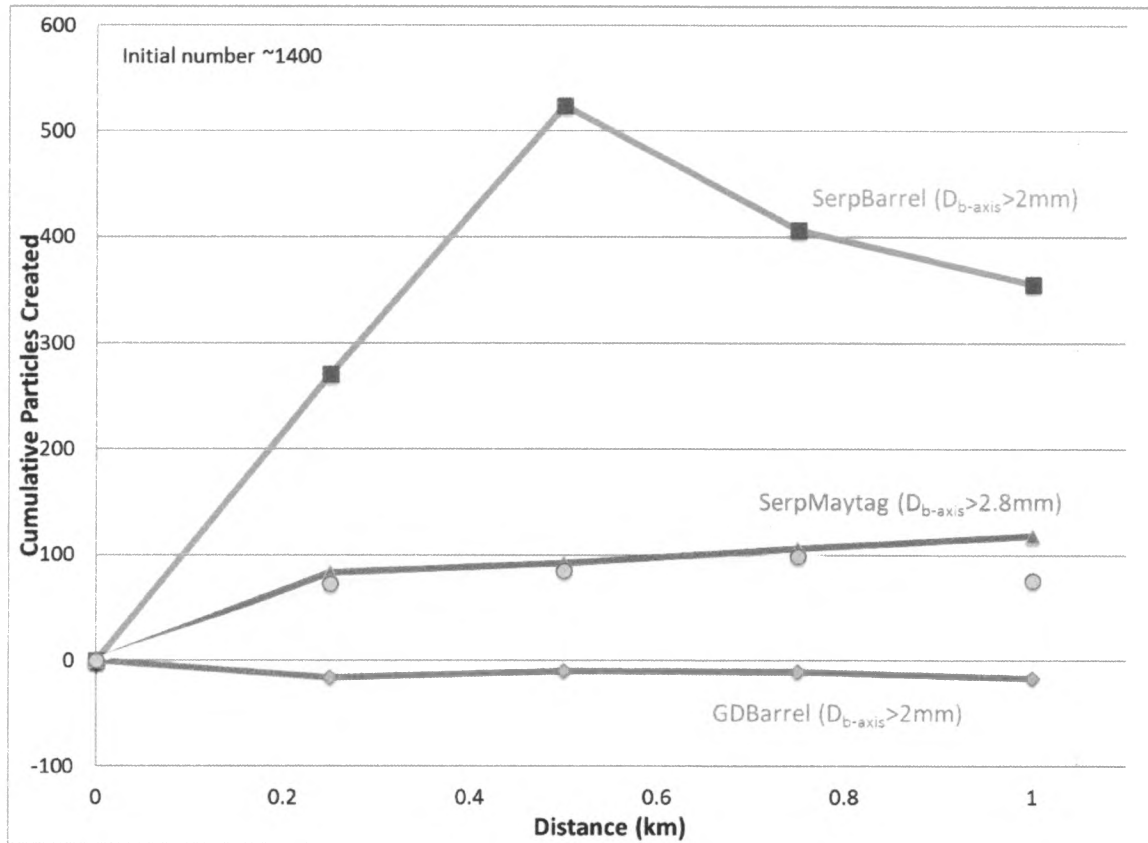
Figure 16: Comparison of number of particles created for this study (SerpBarrel and SerpMaytag) with Arabnia and Sklar, 2016 (GDBarrel and GDMaytag).
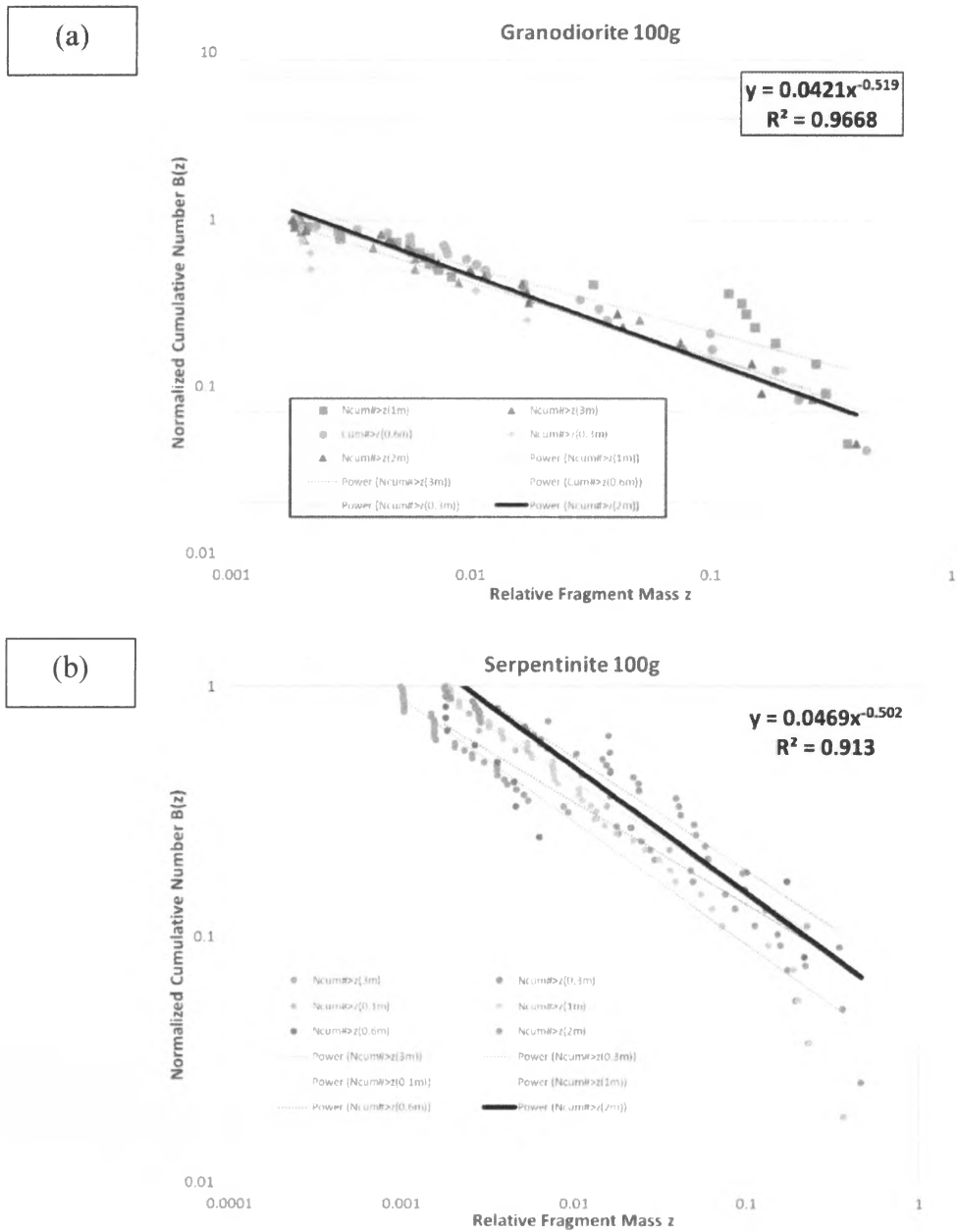
Figure 17: Fit parameters for granodiorite (a) and serpentinite (b) used in the code.
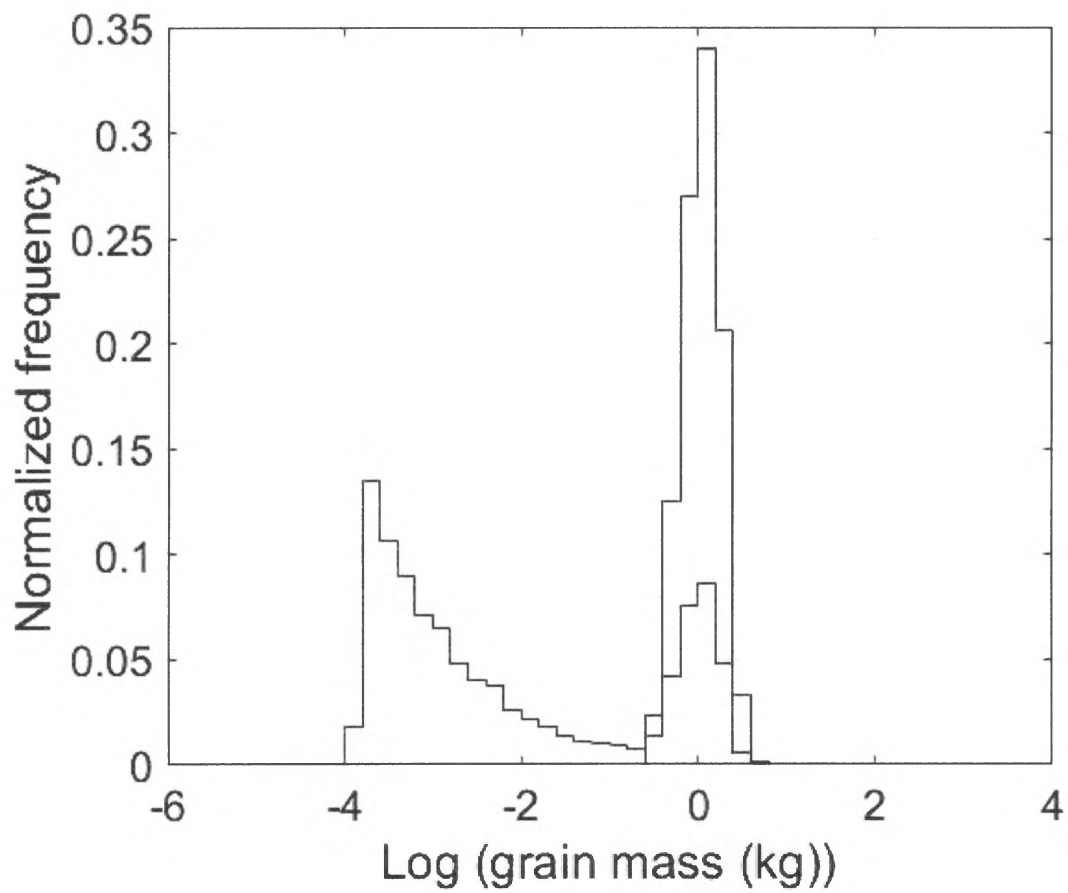
Figure 18: Example model output for PDF for Run1 in the 'Big' drum (4 m) with granodiorite. Before the run is blue, after the run is red. For this simulation, CompNumber = -0.1034 with Impact velocity = 0.6 m/s and ImpactRate = 0.9 impacts/m.
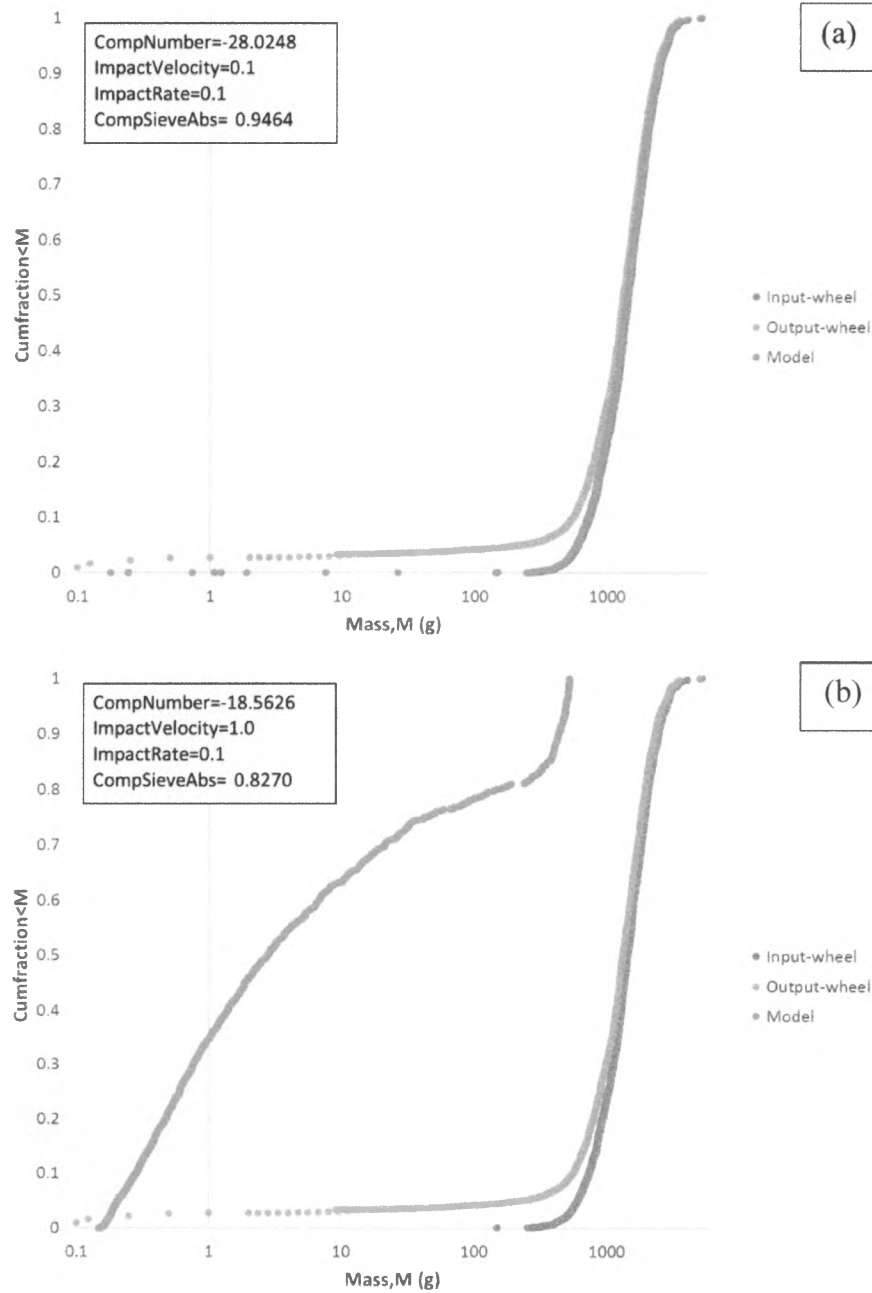
Figure 19: Model versus lab comparison for Run 1 in the 'Big' drum (4 m) considering low impact velocity low impact rate (a) and high impact velocity low impact rate (b).
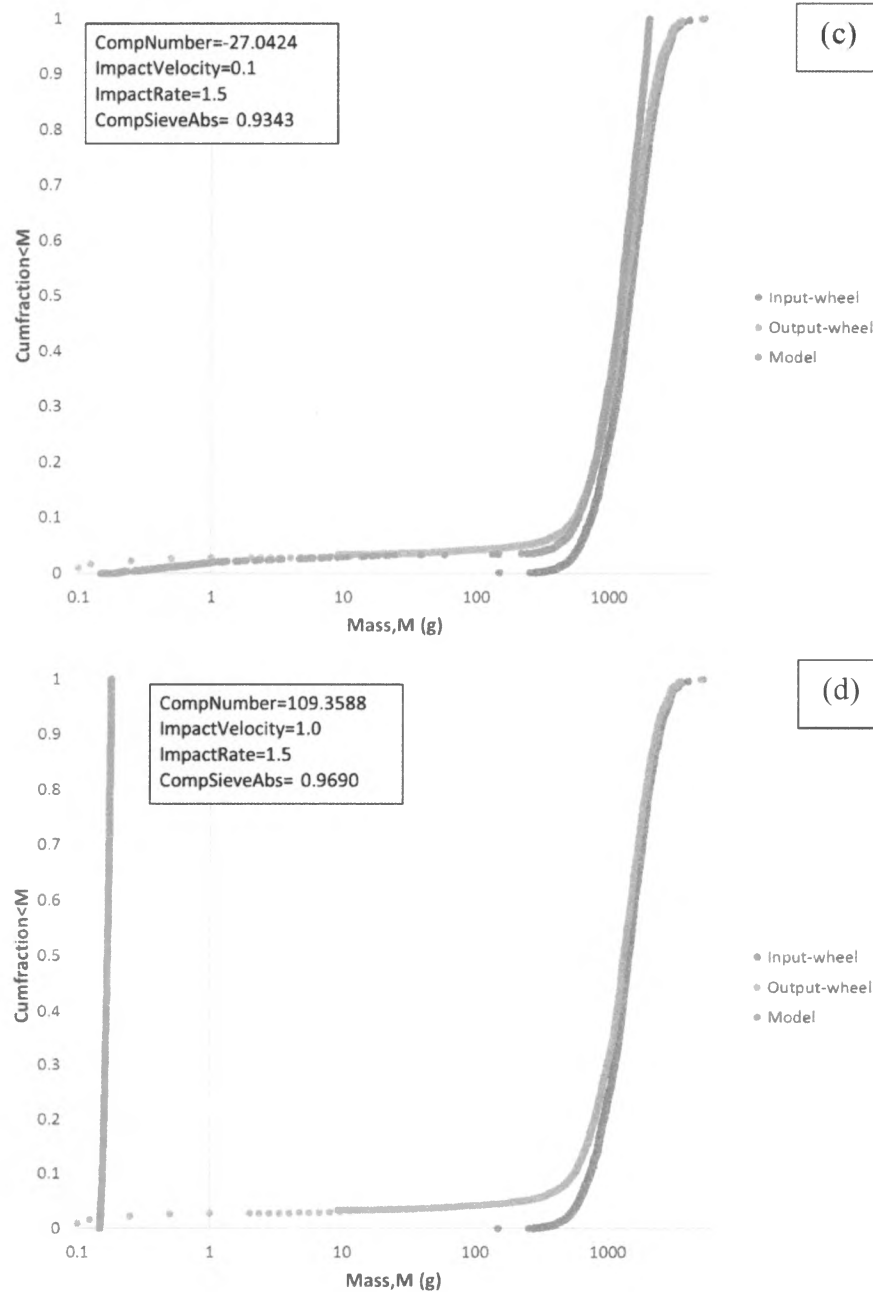
Figure 19: Model versus lab comparison for Run 1 in the 'Big' drum (4 m) considering low impact velocity high impact rate (c) and high impact velocity high impact rate (d).
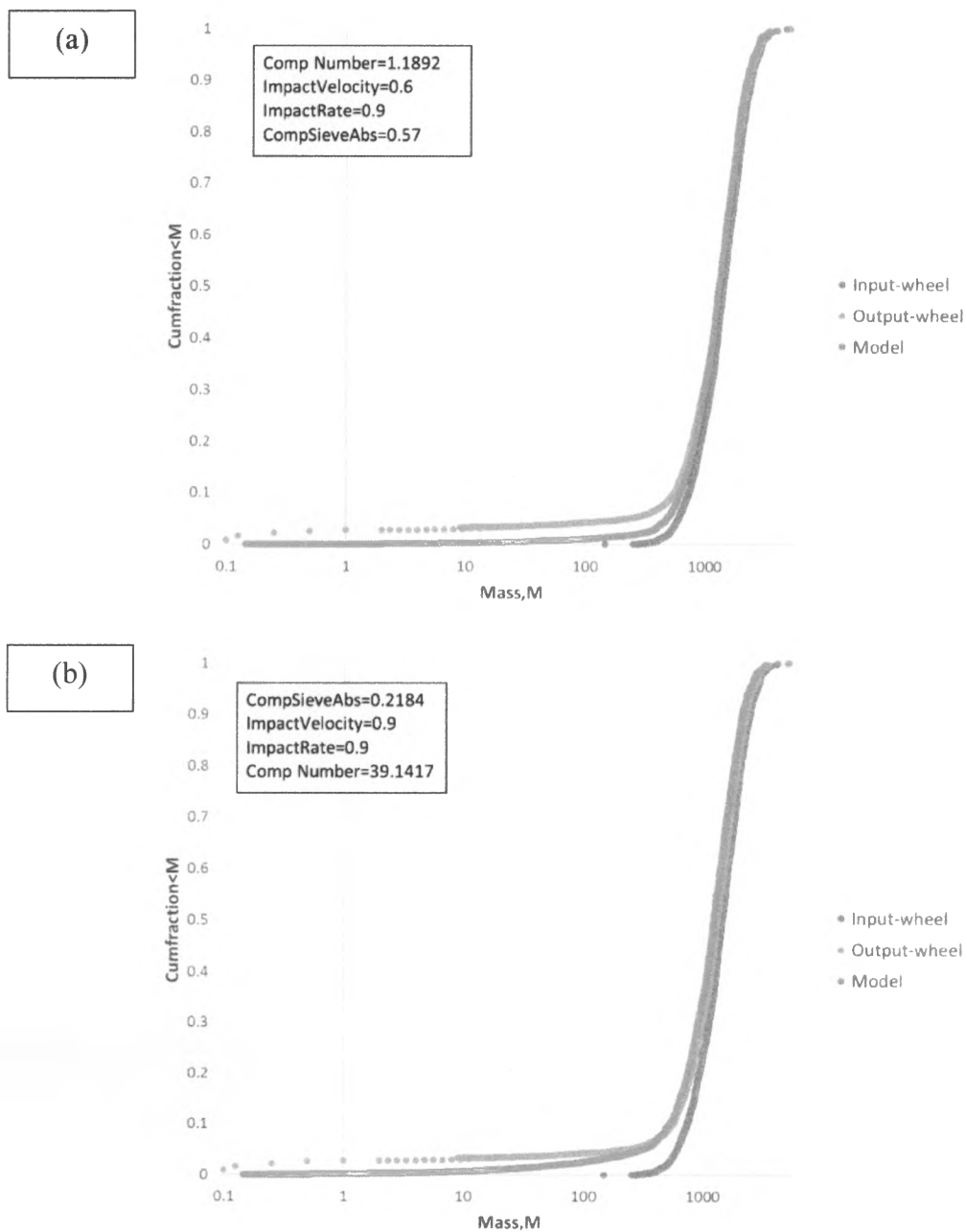
Figure 20: Model versus lab comparison for Run 1 in the 'Big' drum (4 m) considering compNumber (a) and compSieveAbs (b).
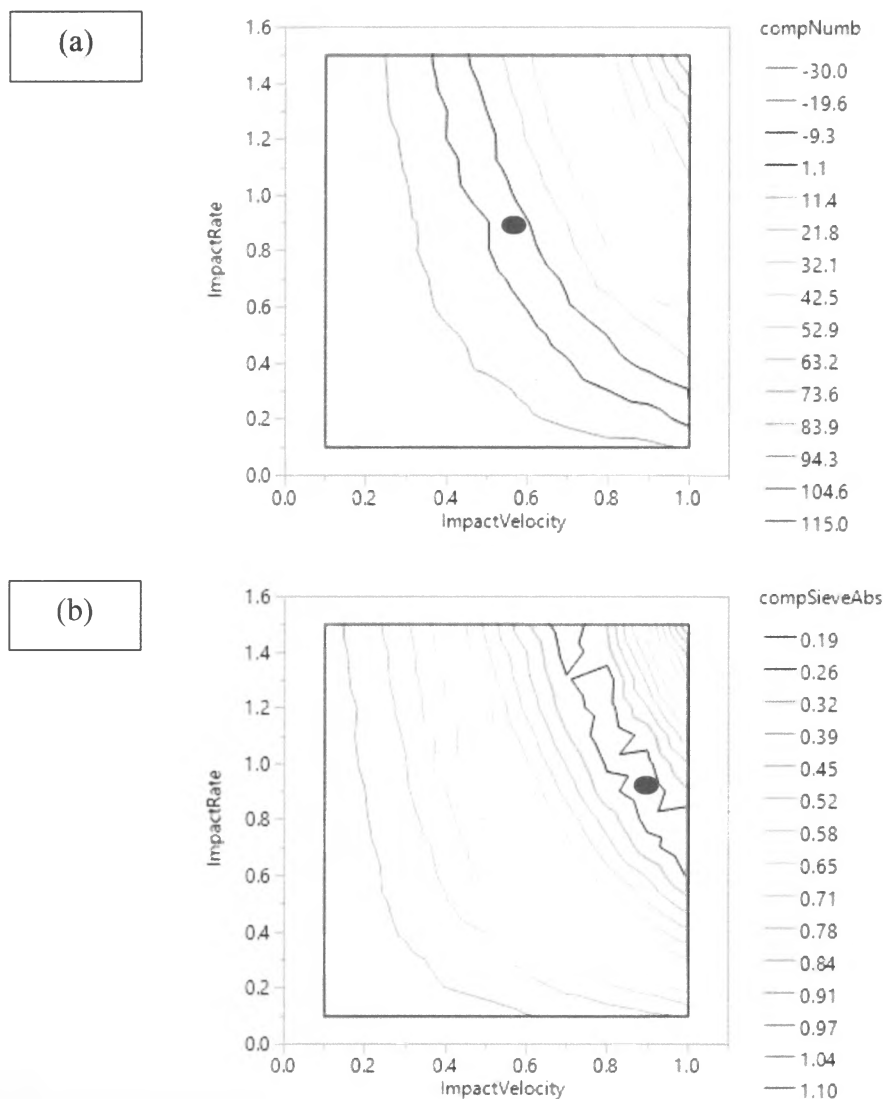
Figure 21: Objective function optimization contour plots for Run1 in the 'Big' drum (4 m) Comp number (a) and compSieveAbs (b). The area within the black contour lines define the optimum values and the red dots indicate the values for impact velocity and impact rate used in Figure 20.
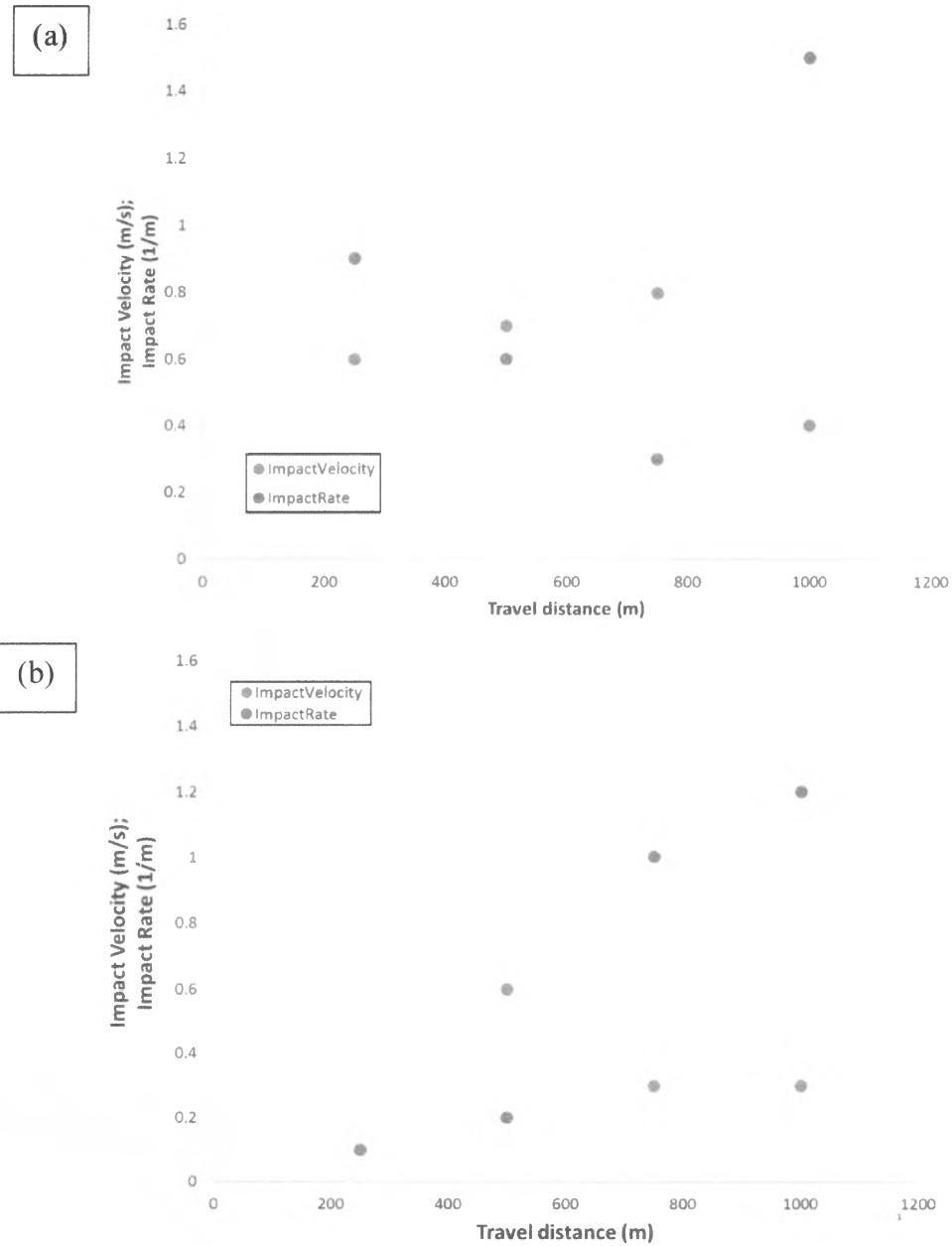
Figure 22: Optimum parameters plots for compNumber with 'Big' drum (4 m) data (a), 'Dawdy' drum (1.65 m) data (b).
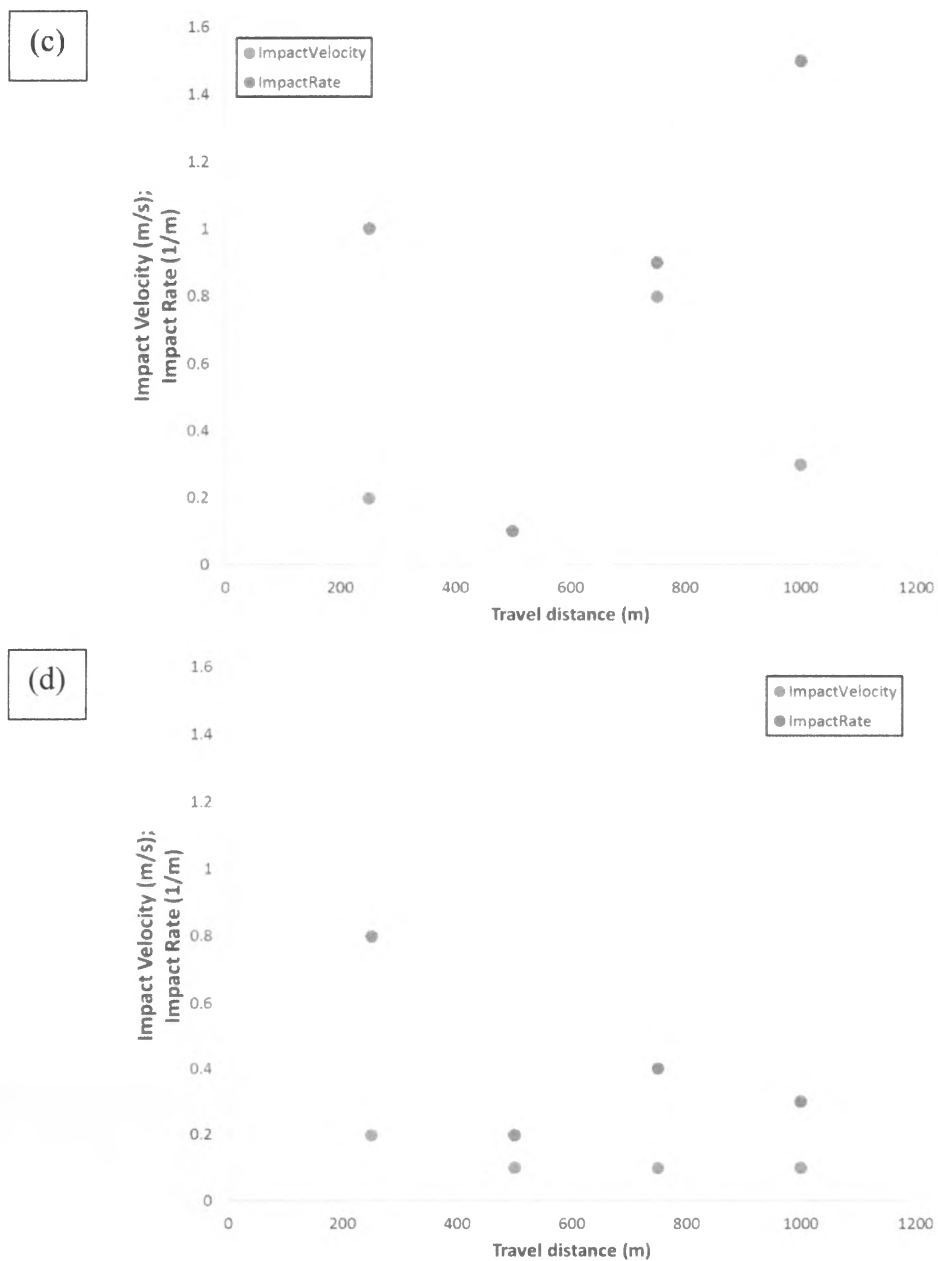
Figure 22: Optimum parameters plots for compNumber 'Maytag' drum (0.56 m) granodiorite data (c), and 'Maytag' drum (0.56 m) serpentinite data (d).
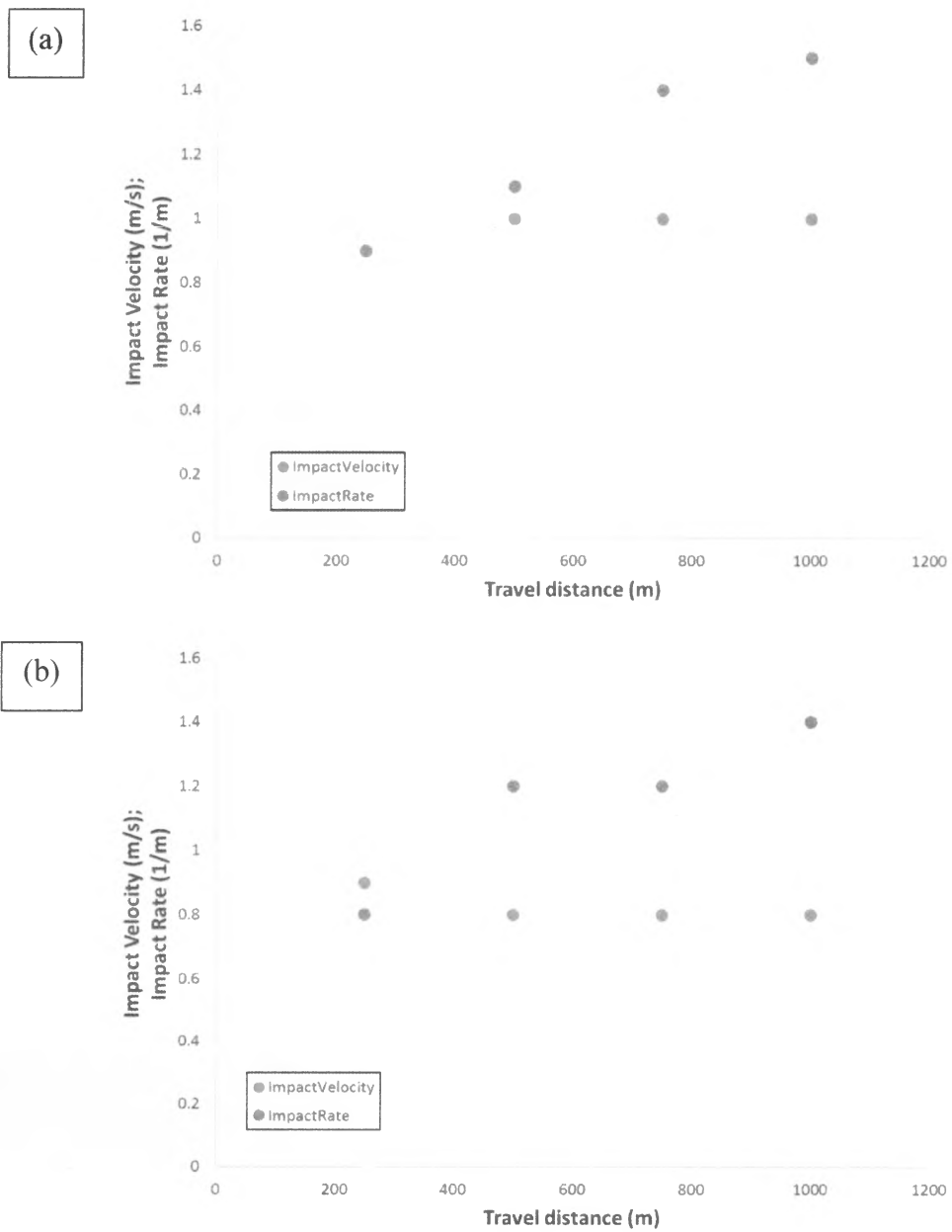
Figure 23: Optimum parameters plots for compSieveAbs with 'Big' drum (4 m) data (a), 'Dawdy' drum (1.65 m) data (b).
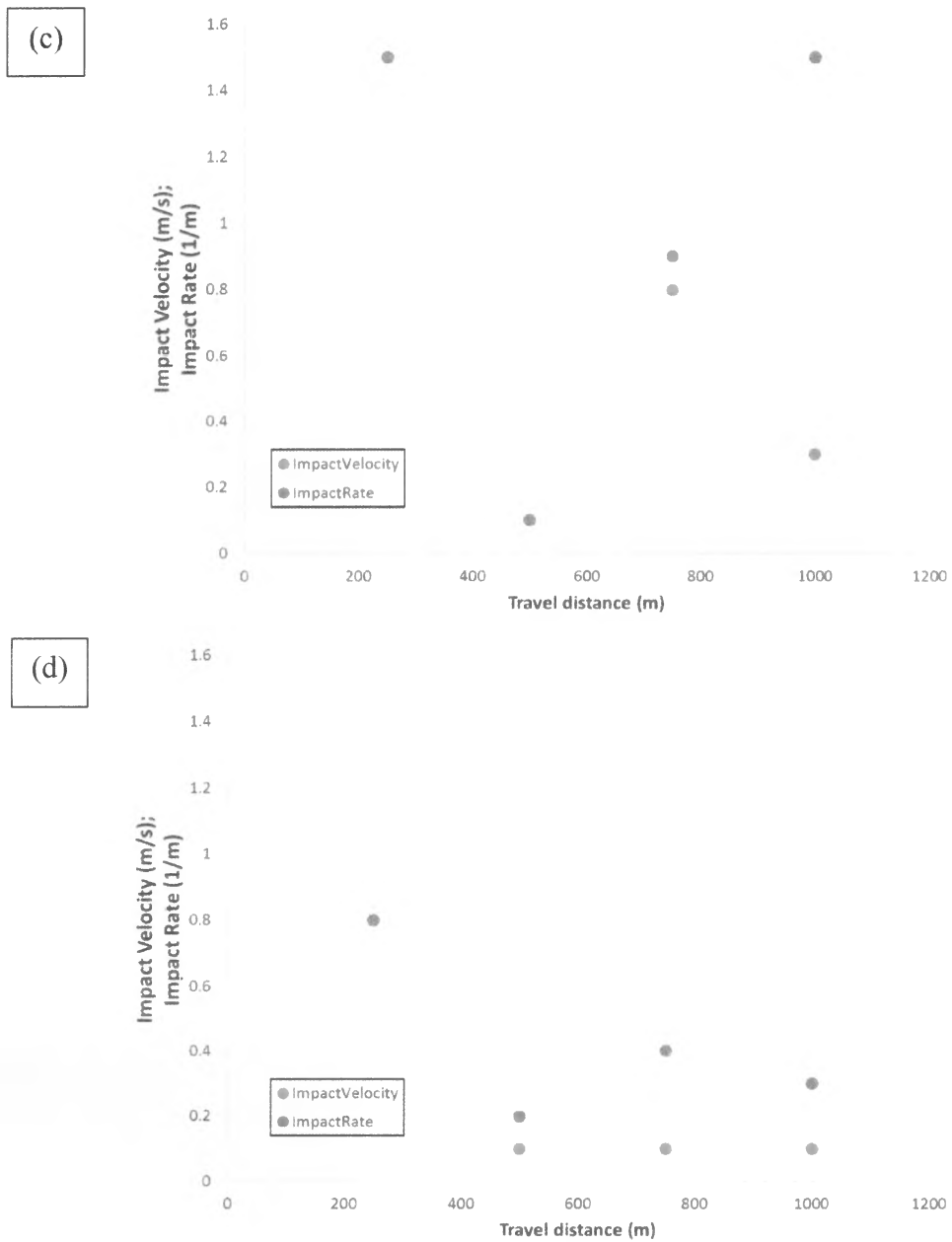
Figure 23: Optimum parameters plots for 'Maytag' drum (0.56 m) granodiorite data (c), and 'Maytag' drum (0.56 m) serpentinite data (d).
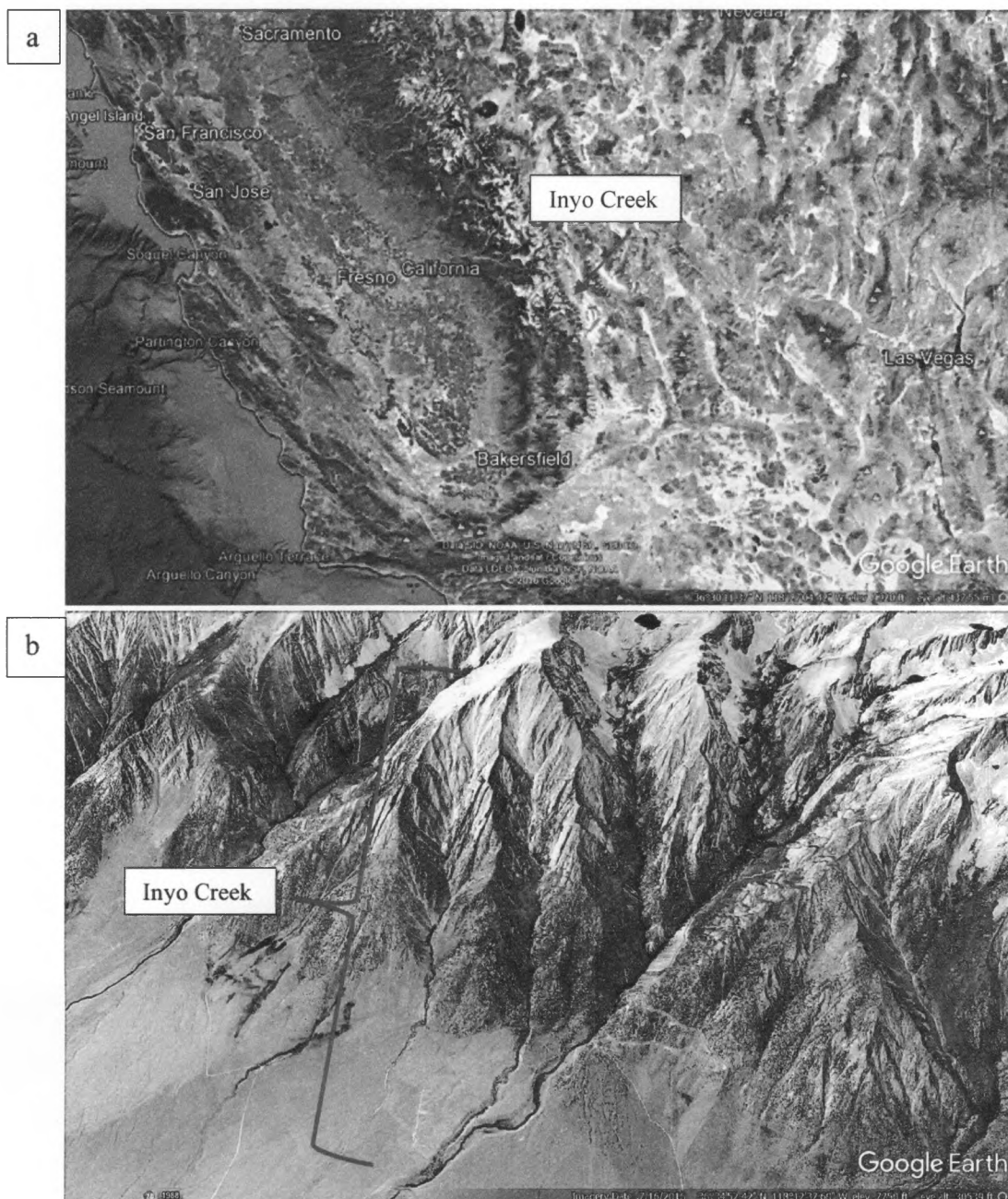
Figure 24: Google Earth generated images showing Inyo Creek location in the eastern Sierra Nevada (a) and the general geomorphology of the area (b).
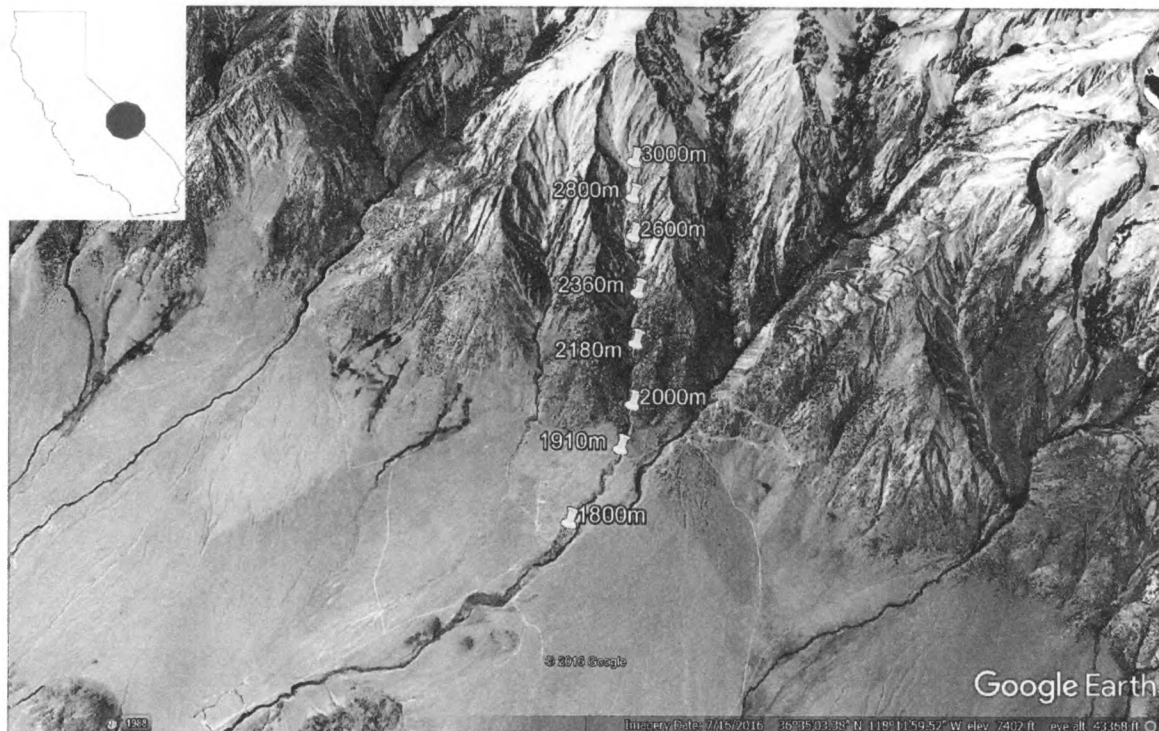
Figure 25: Field location map. The elevation indicates where I collected "slack water" samples within the watershed of Inyo Creek. Some of the 11 sites are not represented in the figure because of graphic reasons.
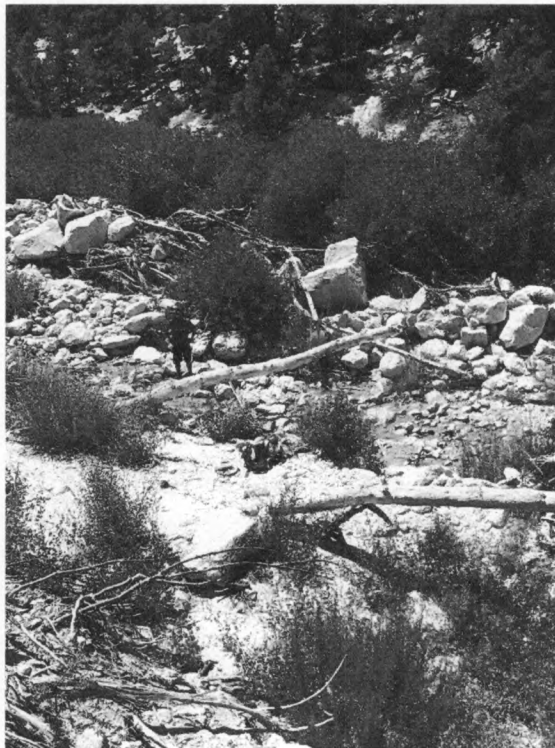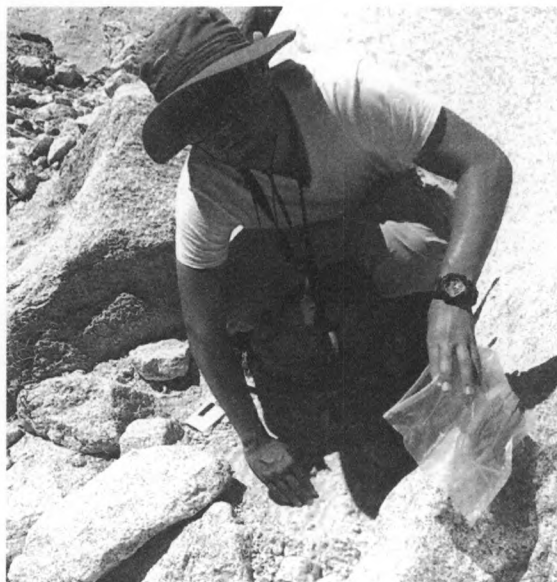
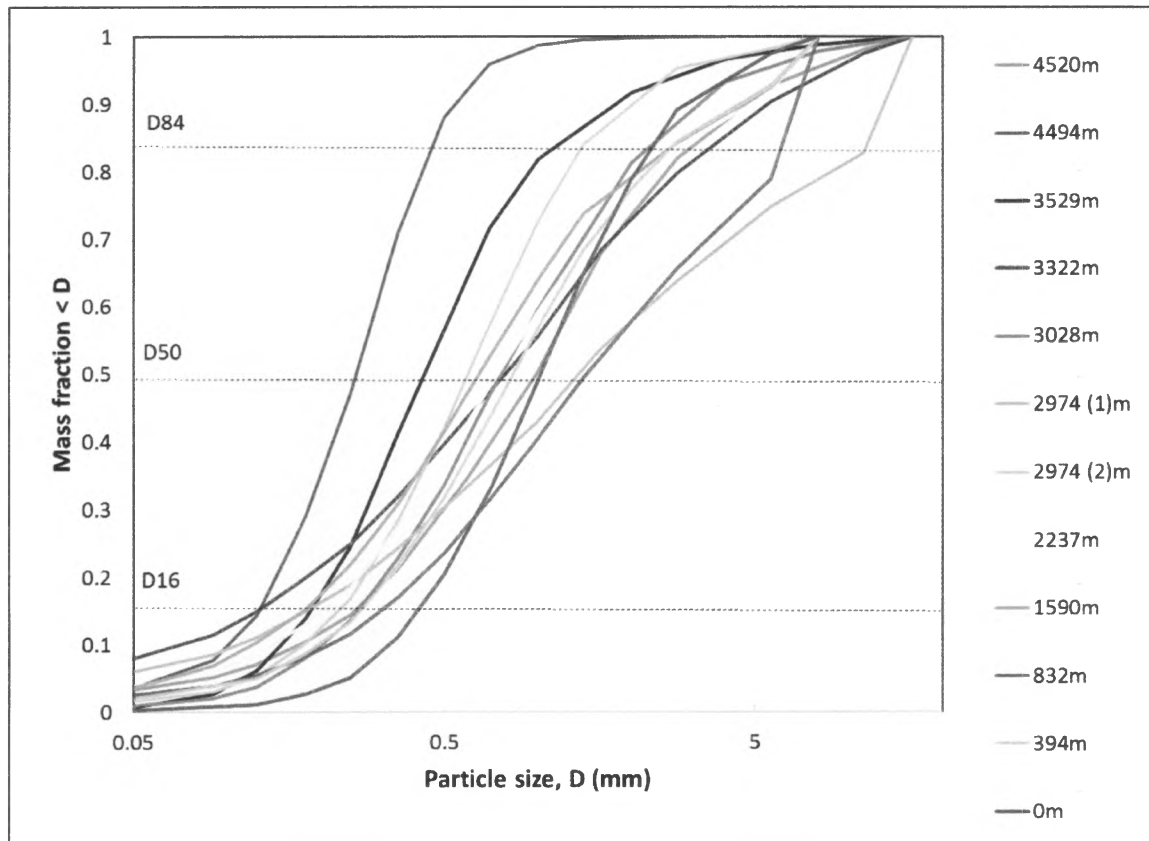Figure 26: Field site 2180 m for slack water sampling. Geomorphic setting (a), collection site (b).

Figure 27: Cumulative particle size distributions for slack water samples collected at Inyo Creek. The legend is referring to travel distance from the upstream-most sampling point at 3000 m elevation. Elevation 2974 m shows two samples because I found an extensive area with different visible particle size.
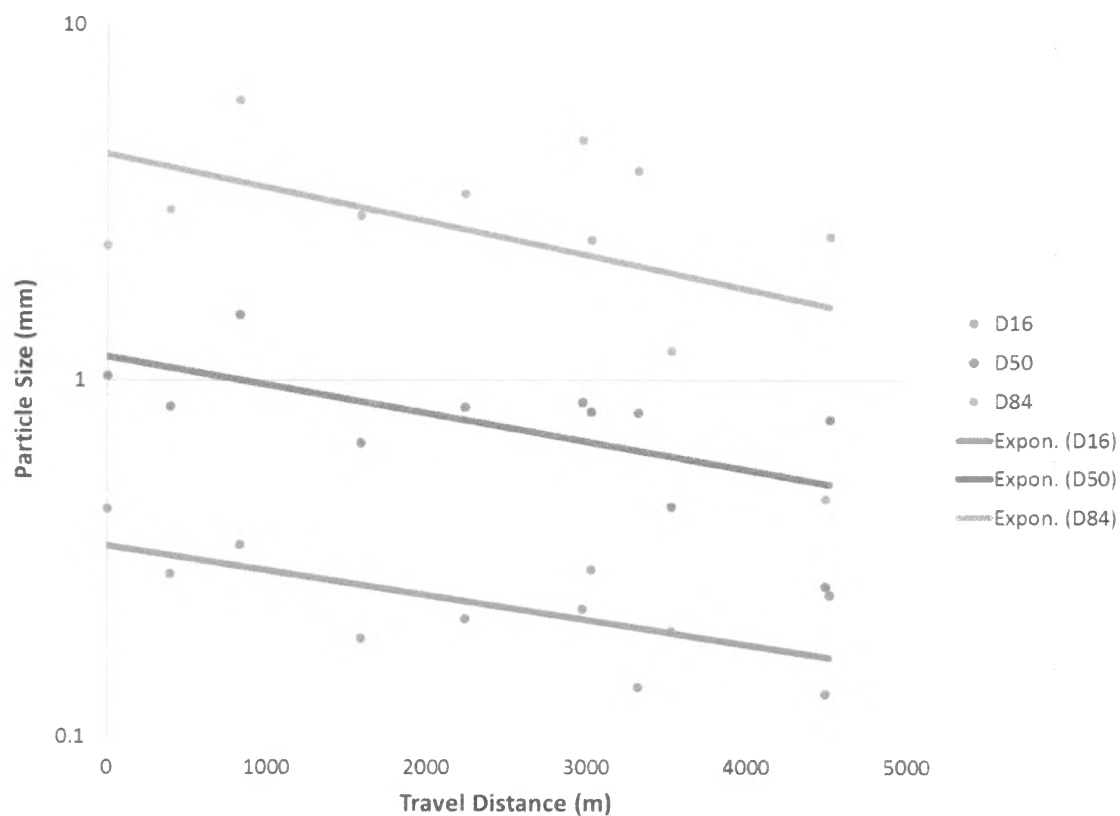
Figure 28: Particle size as a function of travel distance for slack water samples collected at Inyo Creek. Quantiles of the distributions include D16, D50, and D84. Also shown are exponential fits for the data points.
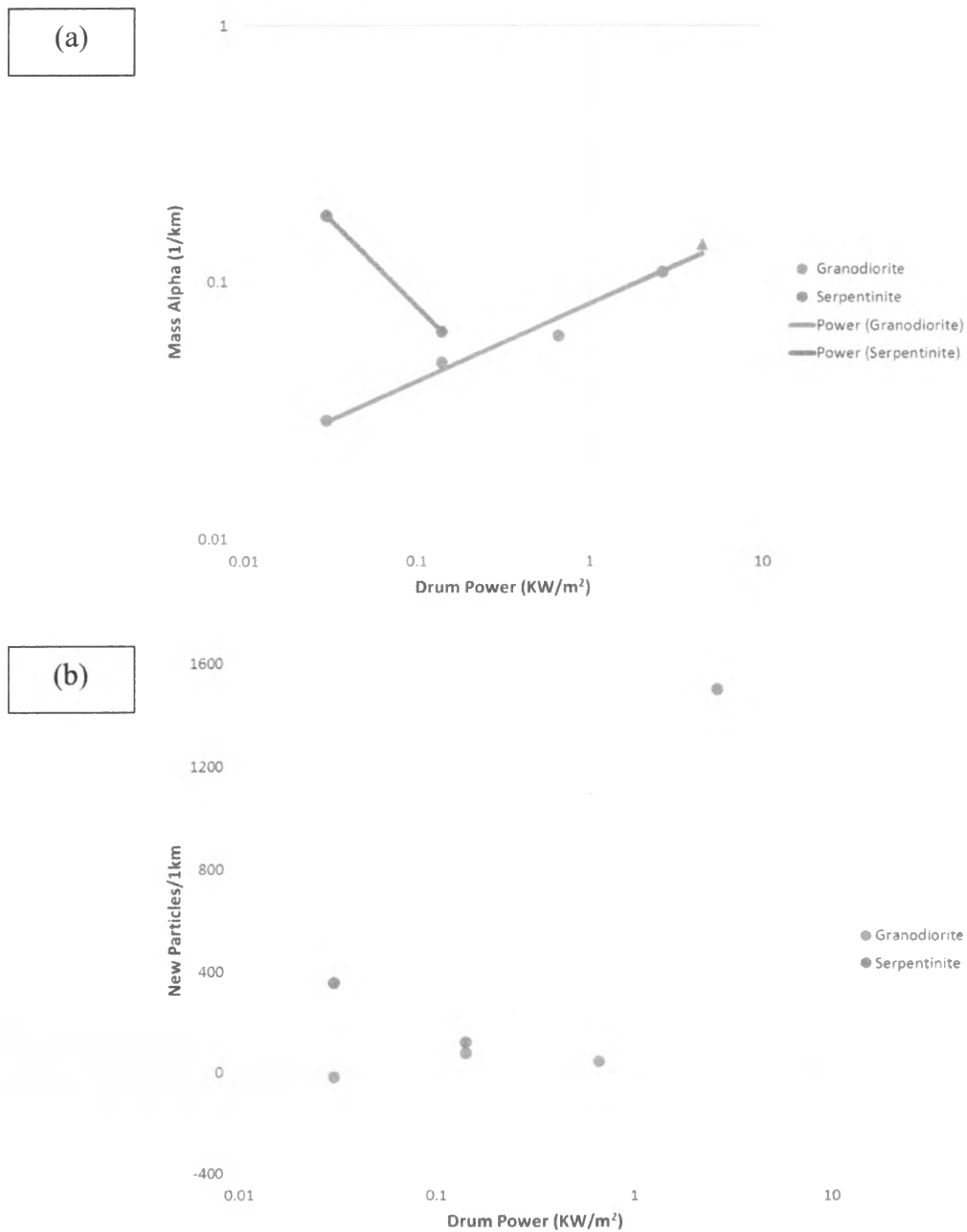
Figure 29: Drum power versus Mass Alpha (a) and Drum Power versus new particles created over a km (b). The triangle in (a) represents the prediction for Inyo Creek.
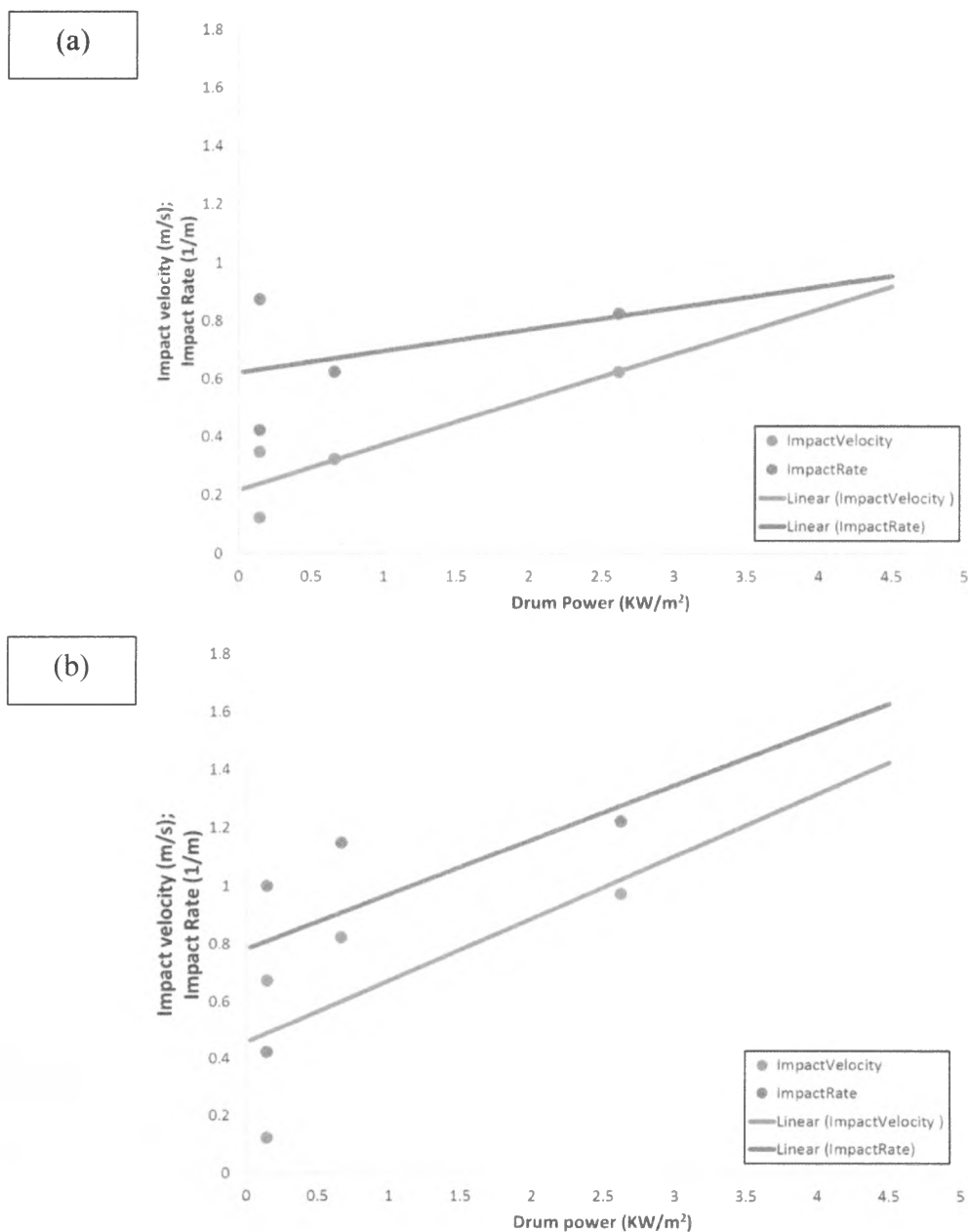
Figure 30: Drum power versus Impact velocity/rate with averages from compNumber (a) and compSieveAbs (b).